Higher Order Non-Oscillatory Schemes in Ideal Magnetohydrodynamics

M.Tech. (Dual Degree) Project Dissertation

by

Debojyoti Ghosh
01D01010

Under the guidance of

## Prof. Avijit Chatterjee

Department of Aerospace Engineering

Indian Institute of Technology Bombay

June, 2006

Certificate of Approval

Certified that, this dissertation titled "**Higher Order Non – Oscillatory Schemes in Ideal Magnetohydrodynamics**" by **Debojyoti Ghosh (01D01010)**, is approved by us for degree of *Bachelor of Technology* in Aerospace Engineering and *Master of Technology* in Aerospace Engineering with specialization in *Aerodynamics* under the *Dual Degree Program*.

Examiners

Dr. Ajit Kumar Mahendra,
Scientist, B.A.R.C., Mumbai

Prof. Gopal R. Shevare,
Department of Aerospace Engineering

Supervisor

Prof. Avijit Chatterjee
Department of Aerospace Engineering

Chairman

Prof. Rushikesh K. Joshi
Department of Computer Science & Engineering

Date: 30/06/2006
Place: IIT Bombay

Abstract

In recent years, there has been a growing interest in the numerical solution of the MHD system, particularly the idealized system, which is obtained by neglecting dissipative effects. High-resolution schemes, applied successfully to the Euler equations, have been tried for the ideal MHD system. The non-convexity and coincidence of eigenvalues for some conditions raises additional questions regarding the straightforward application of Godunov-type schemes and the admissibility of various non-evolutionary discontinuities. In the present study, the Essentially Non-Oscillatory and the Weighted Essentially Non-Oscillatory class of schemes are applied to the 1D ideal MHD equations. A characteristic-based algorithm is used where the flux vector is resolved along the characteristic directions and reconstructed in an upwinded manner. The algorithm is validated on benchmark 1D problems. The problem of higher order Weighted Non-Oscillatory Schemes showing oscillatory behavior for the ideal MHD system is addressed using a solution-dependent monotonicity-preserving limiting technique which has been proposed in literature. An attempt is made to refine the use of this limiting technique by studying behavior of the constituent characteristic fields of MHD using simplified systems. These systems share the mathematical characteristics of the ideal MHD equations and thus the solutions are expected to be topologically similar. Conclusions drawn from the simplified systems are extended to the ideal MHD system and a selective use of the limiting technique is incorporated to yield a more robust algorithm. Simultaneously, issues regarding the admissibility of MHD waves and pseudo-convergence are studied further and the convergence behavior of the algorithm developed is analyzed. It is seen that the algorithm developed suffers from identical problems of non-uniform convergence as mentioned in literature. Along with these studies, a high-resolution algorithm which uses ENO/WENO-based solution reconstruction is implemented for the 2D MHD system. The flux computation is based on the Roe scheme with the Harten's entropy fix. The code is validated on a range of problems using Cartesian grids and representative results are presented.

Keywords: Ideal Magnetohydrodynamics, ENO, WENO, characteristics, high-resolution schemes, model systems, MP limits, oscillations, pseudo-convergence

Contents

List of Figures

Nomenclature

- **A** - Alfvén wave velocity

- A - Alfvén wave-speed

- $\mathcal{A}, \mathcal{B}, \mathcal{C}$ - Jacobian matrices along x, y and z axes

- **B** - Magnetic flux density

- **B** - Optimum weights of stencils

- **D** - Electric flux density

- **E** - Electric field intensity

- **E** - Total energy of fluid element

- $\mathcal{F}$ - Flux Tensor

- **F** - Numerical Flux

- **H** - Magnetic field intensity

- $\mathcal{I}$ - Identity matrix

- IS - Smoothness indicator of a stencil

- **J** - Current density

- **L** - Left eigenvector in terms of conserved variables

- P^* - Full pressure (Gas pressure + Magnetic Pressure)

- **R** - Right eigenvector in terms of conserved variables

- **S** - Source term

- S - Stencil for flux computation

- **W** - Primitive variable vector in 2D ($[\rho,\ u,\ v,\ w,\ B_x,\ B_y,\ B_z,\ p]^T$)

- a - Speed of sound

- c - A constant for the model systems

- c_a, c_f, c_s - MHD wavespeeds

- d - Curvature measure at cell or interface

- e - Fluid internal energy

- **f, g, h** - Flux vectors in Cartesian coordinate directions

- f - Decoupled flux vector component

- $\hat{\mathbf{k}}$ - Unit wave propagation direction vector

- l - Left eigenvector in terms of primitive variables

- $\hat{\mathbf{n}}$ - Unit surface normal

- p - Fluid pressure

- **r** - Right eigenvector in terms of primitive variables

- t - Time

- **u** - Fluid velocity / Conserved variable vector ($[\rho, \ \rho u, \ \rho v, \ \rho w, \ B_x, \ B_y, \ B_z, \ E]^T$)

- u - Component of state vector in model systems / decoupled component of state vector

- v - Component of state vector in model systems

- **w** - Primitive variable vector in 1D ($[\rho, \ u, \ v, \ w, \ B_y, \ B_z, \ p]^T$)

- w - Component of state vector in model systems

- x, y, z - Cartesian coordinates

- $\hat{\mathbf{i}}, \ \hat{\mathbf{j}}, \ \hat{\mathbf{k}}$ - Unit vectors along Cartesian directions

Greek Symbols

- α - LLF constant / weights in WENO

- β - Constant in MP limits construction

- γ - Ratio of specific heats

- ϵ - Electric permittivity / small arbitrary number

- λ - Eigenvalues

- μ - Magnetic permeability

- ∇ - Divergence operator

- ϕ - Terms quantifying dissipative effects in energy equation / Constant in MP limits construction

- ρ - Mass density

- ρ_e - Volume charge density

- ψ - Terms quantifying dissipative effects in momentum equation

- σ - Electric conductivity

- τ_m - Magnetic Stress Tensor

- θ - Rotation angle or angle between wave direction and applied magnetic field

- ω - Angular frequency / weights assigned to stencils in WENO

Subscripts

- L - Left

- R - Right

- a - Alfvén characteristic field

- f - Fast characteristic field

- i, j - Indices for cell / grid point

- k - Index for characteristic field

- n - Component normal to a cell face

- s - Slow characteristic field

- t - Derivative with respect to time

- x - Component along x-axis / derivative with respect to x

- y - Component along y-axis / derivative with respect to y

- z - Component along z-axis

Superscripts

- L - Left

- LC - Large Curvature

- MD - Median

- T - Transpose

- UL - Left-sided upper

- k - Index for characteristic field

- r - Index for stencil in WENO

Abbreviations

- CD - Central Differencing

- CFL - Courant-Friedrich-Levy

- CPU - Central Processing Unit

- CT - Constrained Transport

- EM - Electromagnetic / Electromagnetism

- ENO - Essentially Non-Oscillatory

- LLF - Local Lax-Friedrich

- MHD - Magnetohydrodynamics

- MP - Monotonicity Preserving

- RF - Roe-Fixed

- RK - Runge-Kutta

- TVD - Total Variation Diminishing

- UV - Ultra-violet

- WENO - Weighted Essentially Non-Oscillatory

Chapter 1
Introduction

The equations of ideal magnetohydrodynamics (MHD) describe the flow of a perfectly conducting, inviscid fluid in the presence of a magnetic field [1, 2]. The dynamics of a conducting fluid can be described by extending the Navier-Stokes equations to include terms for momentum and energy exchange between the fluid elements and the electromagnetic field. The evolution of the electric and magnetic fields are governed by the Maxwell's equations of electro-magnetics. The ideal MHD equations are obtained by a series of simplifying assumptions (like perfect conductivity, neglecting dissipative mechanisms and displacement currents, macroscopic neutrality, etc) which are valid for a large class of plasma flows. Thus, they can be viewed as an extension of the Euler equations of gas-dynamics incorporating the momentum and energy terms due to the interaction of fluid elements with the magnetic field. Along with the modified fluid equations, the evolution of the magnetic field is governed by the "induction equation". These equations find application in a wide variety of subjects like controlled fusion reaction [2], the flow of astrophysical jets [3] and flow around hypersonic vehicles [4].

Following the success of Godunov-type schemes in gas-dynamics, these schemes have been applied to the equations of ideal MHD [3, 4, 5, 6, 7]. From the numerical viewpoint, the ideal MHD equations form a non-strict hyperbolic system with a non-convex flux function [5]. In the one-dimensional (1D) system, these equations admit seven eigenvalues where upto five can coincide. The non-convexity of the flux function raises additional questions regarding the admissibility of a class of intermediate waves which are not observed in convex systems like the Euler equations [8, 9, 10, 11, 12]. These issues are yet to be resolved and raises questions regarding the applicability of Godunov-type schemes in ideal MHD. Nevertheless, efforts have been made to solve the ideal MHD equations numerically using information based on the local wave behavior. Brio and Wu [5] introduced an upwind differencing scheme for the 1D system which was based on a Roe-type approximate Riemann solver and demonstrated its superiority over earlier methods. The drawback of their scheme was that a Roe averaged Jacobian could not be found except in the case $\gamma = 2$. Zachary and Collela [6] applied a modification of the Engquist - Osher flux to the equations of 1D MHD. The eigenstructure of the 1D MHD system has also been studied and the eigenvectors proposed by Roe and Balsara [13] have been accepted. Cargo and Gallice [14] outlined the construction of Roe matrices for the ideal MHD system for the general case though their results do not show marked improvements over schemes using simple arithmetic averaging. The insensitivity of the computed flux to the averaged interface state was shown in [13] and thus, most schemes use arithmetic averaging to find the interface state and compute the eigenvalues and eigenvectors. Extension of these 1D schemes to multi-dimensions

have not been straightforward [3, 7] and methods used to ensure the solenoidal nature of the magnetic field have been employed.

The Essentially Non-Oscillatory (ENO) [15, 16, 17] and Weighted Essentially Non-Oscillatory (WENO) [18, 19] family of schemes have been applied to the Euler equations as well as the equations of electro-magnetics with excellent results. Previous attempts have been made to apply the flux-differencing form of the WENO schemes to the MHD system [20, 21] and the results are encouraging. In the present study, the ENO and WENO schemes are applied to the equations of ideal 1D MHD and the performance of these high-resolution schemes are compared for the two coplanar MHD Riemann problems formulated in [5]. The first problem is an extension of the Sod's shock tube with anti-parallel magnetic field and the solution contains a slow compound wave, apart from regular shocks and rarefactions. The second problem is the High Mach number problem, which can be formulated as an equivalent hydrodynamic problem with the full pressure corresponding to the gas pressure [5]. Thus, an analytical solution [6] is possible with which the computed results are compared. The algorithm developed employs characteristic decoupling which decomposes the flux vector into its component along each of the seven characteristic directions. These components are reconstructed using ENO/WENO interpolation and upwinding is done based on the sign of the corresponding eigenvalue. The results computed by the higher order non-oscillatory schemes are compared with the first order upwind scheme and with results presented in literature.

Although the WENO schemes are theoretically expected to exhibit non - oscillatory behavior, numerical experimentation show that higher order WENO schemes show considerable oscillations for certain classes of problems (see discussions in [23]). The WENO class of schemes have been applied to the equations of ideal MHD [20, 23] and in both these studies, oscillatory behavior has been reported for fifth and higher order WENO schemes. Such oscillatory behavior is also seen in the present study and is seen to occur at relatively high CFL numbers. A limiting procedure has been proposed in [24] to alleviate these oscillations where monotonicity preserving (MP) limits are applied to the reconstructed fluxes. The bounds within which the reconstructed value should lie are determined based on the local curvature of the solution. Different curvature measures at the interface have been proposed [24] which differ in their categorization of an oscillation as a genuine extremum or a spurious oscillation. In the present study, an attempt is made to refine the use of these MP limits to the ideal MHD system by isolating specific characteristic fields which contribute to the generation of spurious oscillations. While the results in [23] are encouraging, selective use of the MP limits would result in lower computational cost. To study the behavior of the WENO schemes on specific characteristic fields, the model systems presented in [25, 27] are employed. These models are simplified systems which contain specific waves similar to those in the ideal MHD system and has been used in [25, 26] to study the admissibility of shocks in MHD. Since waves in MHD are symmetric around the fluid velocity, a 3×3 system has been derived in [25] which contain the right-running (with respect to the fluid velocity) waves in MHD (slow, fast and Alfvén). While the Alfvén characteristic field is linearly degenerate, the slow and fast modes are neither linearly degenerate nor genuinely non-linear. This is a result of the non-convex flux function. The reduced system is non-strictly hyperbolic with eigenvalues coinciding like the ideal MHD system and thus, the solutions are expected to be topologically similar to the ideal MHD system. In the present study, the behavior of the Alfvén characteristic field is initially studied using the 2×2 rotationally degenerate system with a cubic flux function [27]. This system consists of two characteristic directions (fast radial and slow angular), one of which is linearly degenerate. The magnetosonic modes (slow and fast) are studied using a set of planar Riemann problems for the 3×3 model system. Since the problems are planar, the Alfvén mode is absent. It is seen that the magnetosonic modes exhibit oscillations when higher order WENO schemes are applied. These oscillations are seen for shocks, rarefactions and compound waves of either family (slow/fast) but the severity differs. Application of the MP limits is seen to alleviate the oscillations and while this is indicative of the requirement of MP limits for the slow and fast characteristic fields in ideal MHD, the efficacy of these limits on the two systems (model and ideal MHD) may differ. The rotationally degenerate model system does not exhibit any oscillations and it can be concluded that the Alfvén mode in ideal MHD does not require any limiting treatment. This is subsequently verified by considering non-planar Riemann problems of the 3×3 model system. Based on these observations, the characteristic-based algorithm developed for the 1D ideal MHD equations is modified to incorporate MP limits on the magnetosonic and entropy modes and its performance is evaluated on benchmark 1D Riemann problems (Brio & Wu's shock tube [5] and High Mach No. problem [5, 6]). Additionally, non-planar modifications of the Brio & Wu's shock tube (similar to those considered in [21]) are solved to study the behavior of the Alfvén mode. The oscillations arising from the higher order WENO schemes are seen to be effectively treated using these limits. As a comparison, the CPU times required for computations with MP limits applied to selected modes are compared with those with the limits applied to all modes. It is seen that while the use of MP limits increases the computational cost by a considerable amount, there is a significant reduction of computational cost through refining the use of MP limits. These reductions are amplified for finer grids and thus, it is expected that the savings in CPU time will be considerable for extensions to multi-dimensions.

One of the major problems in the straightforward extension of schemes used for the Euler equations to the MHD system arises from the latter's non-convexity. This has led to a debate regarding the admissibility of MHD shocks, which has not been resolved. It is believed by one school of thought that the only physically meaningful shocks are those which are evolutionary in nature, i.e, those across which only one family of characteristics converge [28]. Intermediate shocks, across which more than one family of characteristics converge, are not admitted as physically correct solution. However, it has been shown through numerical computations in [5, 9, 10] that intermediate shocks can exist although the existence of a purely rotational discontinuity is not admissible [25, 26]. Analytical studies as well as astronomical observations have also reported the existence of intermediate shocks. However, the admissibility of such shocks is still questioned since they are non-evolutionary in nature. It has been concluded in [12] that non-evolutionary waves, like intermediate shocks and compound waves disintegrate at

large times to regular shocks and Alfvén waves unless they cause a rotation of the magnetic field by π. Their stability is dictated by their internal structure which depends on the dissipative mechanisms. Thus, intermediate shocks, as seen in the solution of Brio and Wu's shock tube problem, should be allowed in the numerical solutions of the MHD equations. However, one of the pitfalls here is that these shocks depend on the dissipative mechanisms for their properties and thus, any solution containing them will be sensitive to the numerical dissipation in the scheme used. Thus, to capture the correct solution, it is believed by some that inclusion of the dissipative terms for viscosity, resistivity and thermal conductivity is imperative, thereby questioning the practical relevance of the ideal MHD equations. These issues are intrinsically related to the occurrence of "pseudo-convergence", seen for a class of non-planar Riemann problems [21, 22]. This non-uniform convergence has been demonstrated for some special Riemann problems and it has been reported that till a certain level of grid-fineness is reached, the numerical solution seems to converge to an incorrect solution containing non-evolutionary waves like intermediate shocks and compound wave - like structures. These observations have been demonstrated using initial conditions which are small perturbations to non-planar shock tube problems. In the present study, these issues are studied in details for the 1D algorithm developed.

Simultaneously, the 1D algorithm is extended to 2D. This has necessitated the use of the 8-wave formulation [3, 29] to maintain the solenoidal nature of the computed solution, thereby resulting in non-conservative governing equations. Presently, a higher-order extension of the Roe's scheme using ENO/WENO reconstruction is implemented where the components of the decoupled state vector (characteristic variables) are reconstructed using the 2nd and 3rd order ENO and the 5th order WENO schemes. The state vector and the flux are reconstructed using higher order interpolation via characteristic decoupling. A number of test cases have been solved for to validate the the code and these include hydrodynamic Riemann problems [30], oblique shock reflection problem, blast wave problem (with and without magnetic field) [31], the rotor problem [32], the cloud-shock interaction problem [32] and the Orszag-Tang vortex problem [7]. Representative results are presented.

Chapter 2
Plasma Dynamics and Ideal Magnetohydrodynamics

A large variety of electrically conducting fluids which are neutral on the macroscopic scale are defined by the term *plasma*. A collection of free electrons and ions have to satisfy certain criteria [1, 2] to qualify as a plasma. One of the features of plasmas is that they exhibit a collective behavior with the each particle motion governed by the coulombic and magnetic fields due to surrounding particles as well as external fields. It is often thought of as the fourth state of matter. At high temperatures, the atoms in gases ionize due to collisions since the thermal kinetic energy is enough to overcome the binding energy of outer electrons. One distinguishing feature is that the transition from the gaseous state to the plasma state is gradual and occurs over a range of temperature, unlike the sharp transition at constant temperature for other phase changes.

The first criterion, which ionized gases have to satisfy to qualify as a plasma is macroscopic neutrality. On a macroscopic scale, it is required that the fluid be electrically neutral. The minimum length scale over which the fluid has to be neutral should be large enough to contain a large number of charged particles but small enough compared to the variations in macroscopic parameters like pressure, density, etc. The maximum length scale over which charge separation may be allowed is called the *Debye length*. It can be estimated from the fact that the potential energy due to the charge separation should not exceed the thermal kinetic energy of the fluid. It ranges from 10^{-4} mm for laboratory plasmas to few meters for interstellar gases. The Debye length is also an estimate of the length scales over which the Coulombic influence of one particle is felt by others. Within this distance (inside the *Debye sphere*), particles arrange themselves so as to shield any electrostatic field inside. The second criterion for definition of plasma is that the number of electrons inside the Debye sphere be very large. The third criterion, which follows from macroscopic neutrality, is that any characteristic length scales in plasma flow should be much larger than the Debye length. Additionally, to ensure electron mobility and thus conductivity, it is required that the average time between electron - neutral particle collisions be much larger than characteristic time scales of the plasma flow (over which physical parameters are varying).

Plasmas can be produced by raising the temperature of a fluid such that a high degree of ionization is obtained. Such plasmas, which are in thermodynamic equilibrium, are found in astrophysical flows. Example of naturally occurring plasmas are the solar plasma, solar wind, the planetary magnetosphere, the ionosphere, etc. Laboratory plasmas are usually produced by photo-ionization (where radiation of frequencies in the UV / X-ray / Gamma rays is used to ionize the fluid) and electric discharge (where strong electric fields are used to energize free

electrons which in turn ionize neutral particles through collision). Some engineering applications of plasmas are thermonuclear fusion reactions, MHD generator and the plasma propelled rocket.

Presently, there are four different theoretical models of plasma dynamics, each with its own set of assumptions, that are used to study various plasma phenomena. These include the kinetic theory, the two-fluid or the particle orbit theory, the statistical approach leading to the many-fluid theory and finally, the magneto-hydrodynamic approximation.

2.1 The Magnetohydrodynamic Approximation

The MHD model is based on the single - fluid, continuum assumption and treats the plasma as a single conducting fluid, having all the normal characteristics of a fluid. It may be composed of many different species (charged and neutral) and the total parameters are the summed / averaged value of the parameters for individual species. Thus, the model is a set of equations governing the evolution of macroscopic variables like density, momentum, energy and the magnetic field. Electrical conductivity of the medium leads to an interaction between the fluid and the electromagnetic (EM) field which have to be accounted for in the momentum and energy conservation equations. Thus, the Navier Stokes equations of fluid dynamics are extended to include terms quantifying the EM force acting on the fluid and energy exchanged between the EM fields and the fluid.

2.1.1 Mass Conservation

The continuity equation is identical to its hydrodynamical counterpart and can be expressed in point form as

$$\frac{\partial \rho}{\partial t} + \nabla.(\rho \mathbf{u}) = 0 \tag{2.1}$$

2.1.2 Momentum Conservation

The total momentum of the particles of plasma is a conserved quantity and changes due to the body forces and surface forces. For a conducting fluid, in addition to fluid pressure and viscosity, fluid elements will experience an electromagnetic body force (an electrostatic force and the Lorentz force) which can be expressed as $\rho_e \mathbf{E} + \mathbf{J} \times \mathbf{B}$. The equation of motion can thus be expressed as

$$\frac{\partial(\rho \mathbf{u})}{\partial t} = \rho_e \mathbf{E} + \mathbf{J} \times \mathbf{B} - \nabla.(p\mathcal{I} + \frac{1}{2}\rho\mathbf{u}\mathbf{u}) + \psi \tag{2.2}$$

where $\mathcal{I}$ is the 3×3 identity matrix and ψ is the viscous term.

2.1.3 Energy Conservation

For a volume moving with the fluid, enclosing the same amount of fluid, the rate of increase in energy is sum of the rate of change in the kinetic energy ($\frac{1}{2}\rho\frac{Du^2}{Dt}$) and the rate of change in

internal energy ($\rho\frac{De}{Dt}$). This change has to be balanced by the energy inputs which are primarily from three sources: rate at which the electromagnetic energy enters the volume ($\mathbf{E}.\mathbf{J}$), energy entering through heat conduction and diffusion of species and the rate at which the surface forces of pressure and viscosity does work. Thus, the equation for energy conservation can be expressed as

$$\frac{1}{2}\rho\frac{Du^2}{Dt} + \rho\frac{De}{Dt} = -p\nabla.\mathbf{u} + \mathbf{E}.\mathbf{J} + \phi \tag{2.3}$$

where ϕ represents terms related to heat conduction, diffusion and work done by viscous forces.

2.1.4 Maxwell's Equations

In addition to the three equations governing the evolution of fluid parameters, the evolution of the electromagnetic fields is governed by the Maxwell's equations, which can be expressed as:

$$\frac{\partial \mathbf{B}}{\partial t} + \nabla \times \mathbf{E} = 0 \tag{2.4}$$

$$\frac{\partial \mathbf{D}}{\partial t} - \nabla \times \mathbf{H} + \mathbf{J} = 0 \tag{2.5}$$

$$\nabla.\mathbf{D} = \rho_e \tag{2.6}$$

$$\nabla.\mathbf{B} = 0 \tag{2.7}$$

supplemented by the equation for charge conservation, which can be expressed as:

$$\frac{\partial \rho_e}{\partial t} + \nabla.\mathbf{J} = 0 \tag{2.8}$$

and the generalized Ohm's law which can be expressed as

$$\mathbf{J} = \sigma(\mathbf{E} + \mathbf{u} \times \mathbf{B}) \tag{2.9}$$

The system consisting of eqs. (2.1) to (2.9) is the complete magneto-hydrodynamic system, which is the counterpart of the Navier - Stokes equation for fluid dynamics.

2.2 Simplifications and the Ideal MHD Equations

When applied to practical cases, the complete MHD system, represented by eqs. (2.1) to (2.9) are never used. A number of approximations and assumptions are used to simplify the system and obtain the ideal MHD equations. One of the approximations used is the neglecting of the displacement current, compared to the conduction current. For a sinusoidal variation of $\mathbf{E}$, the ratio of amplitudes of the displacement current with the conduction current can be found as

$$\frac{\epsilon(\partial \mathbf{E}/\partial t)_{max}}{\sigma \mathbf{E}_{max}} = \frac{\epsilon\omega}{\sigma} \approx 10^{-13}\omega \tag{2.10}$$

Thus, for low frequency phenomena (for frequencies not higher than the microwave range), the displacement current can be neglected. Also, by the criterion of macroscopic neutrality of

plasma, the free charge density ρ_e can be assumed to be zero. Thus, current flow due to flow of free charge ($\rho_e \mathbf{u}$) can be neglected compared to the conduction current. Also, the electrostatic body forces can be neglected compared to the magnetic forces.

In addition to these assumptions, the dissipative mechanisms like viscosity, thermal conductivity, diffusion and electrical resistivity are neglected. Assumption of the fluid being a perfect electric conductor results in the simplification

$$\mathbf{E} = -\mathbf{u} \times \mathbf{B} \tag{2.11}$$

With these simplifications, the ideal MHD system can be obtained as [1, 2]:

$$\rho_t + \nabla.(\rho\mathbf{u}) = 0 \text{ (Mass conservation)}$$
$$(\rho\mathbf{u})_t + \nabla.(\rho\mathbf{u}\mathbf{u} + P^*\mathcal{I} - \frac{\mathbf{B}\mathbf{B}}{\mu}) = 0 \text{ (Momentum Conservation)}$$
$$\mathbf{B}_t + \nabla.(\mathbf{u}\mathbf{B} - \mathbf{B}\mathbf{u}) = 0 \text{ (Induction Equation)}$$
$$E_t + \nabla.[(E + P^*)\mathbf{u} - \frac{1}{\mu}(\mathbf{u}.\mathbf{B})\mathbf{B}] = 0 \text{ (Energy Conservation)} \tag{2.12}$$

where $P^* = p + \mathbf{B}.\mathbf{B}/2\mu$ is the full pressure (defined as the sum of gas pressure and the magnetic pressure) and $E = \rho\mathbf{u}.\mathbf{u}/2 + p/(\gamma-1) + \mathbf{B}.\mathbf{B}/2\mu$ is the total energy of the system. Additionally, the divergence free condition $\nabla.\mathbf{B} = 0$ needs to be satisfied. Theoretically, if the initial conditions satisfy this constraint, then the solution at all time satisfies it. However, in numerical computations, small errors can arise which causes non-zero divergence of the magnetic field. These considerations are important while solving multi-dimensional problems.

2.3 Effect of a Magnetic Field

One of the ways of understanding the effect of the magnetic field is through the magnetic stress tensor. From the momentum equation of the ideal MHD system, eq. (2.12), it is seen that the magnetic force can be expressed as the gradient of the magnetic stress tensor which can be expressed as

$$\mathcal{T}_m = \frac{1}{\mu}(\mathbf{B}\mathbf{B} - \frac{1}{2}B^2\mathcal{I}) \tag{2.13}$$

which can be expressed in matrix form as

$$\mathcal{T}_m = \frac{1}{\mu}\begin{bmatrix} (B_x^2 - B^2/2) & B_xB_y & B_xB_z \\ B_yB_x & (B_y^2 - B^2/2) & B_yB_z \\ B_zB_x & B_zB_y & (B_z^2 - B^2/2) \end{bmatrix} \tag{2.14}$$

Assuming a local coordinate system, where the z-axis is aligned with the magnetic field ($\mathbf{B} = B\hat{\mathbf{z}}$), the principal stresses can be obtained as

$$\mathcal{T}_m = \frac{1}{2\mu}\begin{bmatrix} -B^2 & 0 & 0 \\ 0 & -B^2 & 0 \\ 0 & 0 & B^2 \end{bmatrix} \tag{2.15}$$

which can be expressed as

$$\mathcal{T}_m = \frac{1}{\mu}\begin{bmatrix} 0 & 0 & 0 \\ 0 & 0 & 0 \\ 0 & 0 & B^2 \end{bmatrix} + \frac{1}{2\mu}\begin{bmatrix} -B^2 & 0 & 0 \\ 0 & -B^2 & 0 \\ 0 & 0 & -B^2 \end{bmatrix} \tag{2.16}$$

Thus, the effect of the magnetic force on the fluid element is an isotropic *magnetic pressure* of $B^2/2\mu$ and a tension of B^2/μ along the magnetic field lines. The magnetic pressure can be added with the fluid pressure to give the *full pressure*.

Another effect of the magnetic field in a highly conducting medium is the freezing of the field lines to the fluid. This implies that the magnetic field lines move along exactly with the fluid. This can be mathematically proved from induction equation of the ideal MHD system, eq. (2.12), by considering the conservation of magnetic flux through a small surface whose each point moves with the local flow velocity [2]. Thus, any motion along the magnetic field lines is not restricted while any motion perpendicular to them carries them along. This is expected, since any perpendicular motion will cause an induced electric field $-\mathbf{u} \times \mathbf{B}$. For a fluid with infinite conductivity, this implies that the perpendicular velocity component be infinitesimally small so that the current remains finite.

2.4 MHD Waves

While in the case of a non - conducting fluid the only type of wave motion possible is the longitudinal sound wave, a conducting fluid immersed in a magnetic field admits other types of wave motions. It has been seen in the previous section that the effect of an external magnetic field B is an isotropic pressure of $B^2/2\mu$ as well as a tension of B^2/μ acting along the magnetic field lines. Thus, fluid elements along the magnetic field lines behave in a manner similar to a string under tension. Thus, an additional mode of wave propagation, which is the transverse mode, called the *Alfvén wave* is possible in this case. The speed of wave propagation along the direction of the magnetic field can be found as:

$$A = \sqrt{\left(\frac{tension}{density}\right)} = \sqrt{\frac{(\mathbf{B}^2/\mu)}{\rho}} \tag{2.17}$$

which is known as the Alfvén speed. In this mode of propagation, the fluid velocity and the magnetic field components transverse to the field lines vary with time, while all other properties remain constant.

Longitudinal waves, also known as *magneto-sonic* or *magneto-acoustic* waves, occurring in such fluids differ in nature depending on the direction of wave propagation. It has been seen that the magnetic field lines are frozen in the fluid and thus, any fluid motion perpendicular to the field lines cause the field lines to move with the fluid. Thus, when the direction of propagation is along that of the magnetic field, the waves are identical to pure sound waves, causing no perturbation to the magnetic field. Expectedly, the speed of propagation is that
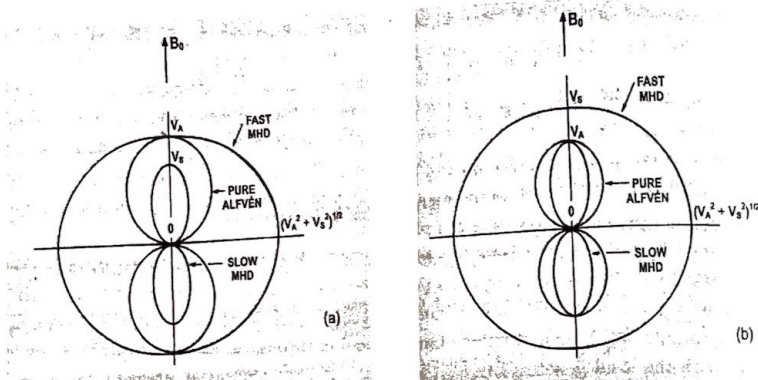
Figure 2.1: Variation of MHD wavespeeds with angle: (a) Speed of sound lesser than Alfven speed (b) Speed of sound greater than Alfven speed [2]

of sound ($a = \sqrt{\gamma p / \rho}$). Perpendicular to the magnetic field, the wave propagation causes the magnetic field lines to compress and rarefact along with the pressure and density. The wave-speed for this motion can be derived by considering the full pressure (sum of fluid and magnetic pressure) and can be expressed as:

$$V = \sqrt{\frac{\gamma p}{\rho} + \frac{(\mathbf{B}^2/\mu)}{\rho}} = \sqrt{a^2 + A^2} \qquad (2.18)$$

Thus, parallel to the magnetic field, there are two waves propagating: the transverse Alfvén wave and the longitudinal sound wave; while perpendicular to the field, there is only one type of wave motion, the longitudinal magneto-acoustic wave.

In any arbitrary direction, the MHD equations for small perturbations to the steady state yields three solutions. One of them is the Alfvén wave, which carries the perturbations normal to the plane defined by the external magnetic field and the direction of propagation. Thus it is a transverse wave and its wavespeed is seen to be

$$c_a = \mathbf{A}.\hat{\mathbf{k}} = \frac{B\cos\theta}{\sqrt{\rho\mu}} \qquad (2.19)$$

where $\mathbf{A} = \mathbf{B}/\sqrt{\mu\rho}$ is the *Alfvén velocity* while $\hat{\mathbf{k}}$ is the direction of propagation of the wave and θ is the angle between the wave propagation direction and the applied magnetic field. For propagation along the field, this reduces to eq. (2.17) while for propagation normal to the field, this mode does not exist. The other two modes constitute a system of coupled waves through which quantities line the pressure, density and in-plane components of magnetic field and velocity vary. These are known as the *slow* and *fast MHD waves*. The wavespeeds of these

modes are given by

$$c_{f,s}^2 = \frac{1}{2}[(a^2 + A^2) \pm \sqrt{(a^2 + A^2)^2 - 4a^2 A^2 \cos^2\theta}] \qquad (2.20)$$

where '+' corresponds to the fast wave while '−' corresponds to the slow wave.

If the Alfvén speed is greater (lesser) than the speed of sound, then, parallel to the magnetic field, the fast (slow) wave combines with the transverse wave and the slow (fast) wave behaves as a pure sound wave. Perpendicular to the magnetic field, only the fast MHD wave exists with propagation speed given by eq. (2.18).

Figure (2.1) illustrates the variation of the three wavespeeds with the angle between the magnetic field and propagation direction.

2.5 Computational MHD

Due to the complexity of the MHD system, analytical solutions are not possible except in case of very simple cases. This has led to a growing interest in the numerical solution of these equations. Over the past two decades, a number of numerical schemes have been applied. The eigenstructure of the system has been investigated while different methods have been developed to handle the additional complexities arising from non-convexity and the necessity of ensuring solenoidal magnetic fields.

The ideal MHD system, eq. (2.12), can be written in the conservative form as:

$$\frac{\partial \mathbf{u}}{\partial t} + \nabla.\mathcal{F} = 0 \ \ or \ \ \frac{\partial \mathbf{u}}{\partial t} + \frac{\partial \mathbf{f}}{\partial x} + \frac{\partial \mathbf{g}}{\partial y} + \frac{\partial \mathbf{h}}{\partial z} = 0 \qquad (2.21)$$

where $\mathbf{u}$ is the state vector of dimension eight, consisting of the conserved quantities and $\mathbf{f}$, $\mathbf{g}$ and $\mathbf{h}$ are the flux vectors in the Cartesian directions.

$$\mathbf{u} = \begin{bmatrix} \rho \\ \rho u \\ \rho v \\ \rho w \\ B_x \\ B_y \\ B_z \\ E \end{bmatrix}, \ \mathbf{f} = \begin{bmatrix} \rho u \\ \rho u^2 + P^* \\ \rho uv - B_y B_x \\ \rho uw - B_z B_x \\ 0 \\ uB_y - vB_x \\ uB_z - wB_x \\ (E + P^*)u - B_x(uB_x + vB_y + wB_z) \end{bmatrix},$$

$$\mathbf{g} = \begin{bmatrix} \rho v \\ \rho vu - B_x B_y \\ \rho v^2 + P^* \\ \rho vw - B_z B_y \\ vB_x - uB_y \\ 0 \\ vB_z - wB_y \\ (E + P^*)v - B_y(uB_x + vB_y + wB_z) \end{bmatrix}, \ \mathbf{h} = \begin{bmatrix} \rho w \\ \rho wu - B_x B_z \\ \rho wv - B_y B_z \\ \rho w^2 + P^* \\ wB_x - uB_z \\ wB_y - vB_z \\ 0 \\ (E + P^*)w - B_z(uB_x + vB_y + wB_z) \end{bmatrix}$$

Eq. (2.21) can be written in the quasilinear form as

$$\frac{\partial \mathbf{u}}{\partial t} + (\mathcal{A}, \mathcal{B}, \mathcal{C}).\nabla \mathbf{u} = 0 \qquad (2.22)$$

It has been seen that the 8×8 Jacobian matrices $(\mathcal{A}, \mathcal{B}, \mathcal{C})$ form a non-strictly hyperbolic system, admitting seven eigenvalues representing the entropy wave and the left and right going slow, fast and Alfvén waves with wavespeeds as given in eqs. (2.19) and (2.20). The eighth eigenvalue has the value 0 which is non-physical in nature.

Starting with Brio and Wu [5], a number of high-resolution, upwind schemes have been applied to the 1D system. In 1D, the system reduces to a set of 7 equations, thus giving a 7×7 Jacobian matrix. This is because the divergence free condition on the magnetic field, when applied to the induction equation of eq. (2.12) results in $B_x = constant$. The eigenstructure of this 7×7 system has been extensively studied. The eigenstructure proposed by Jeffrey and Taniuti (*Non-Linear Wave Propagation*, Academic Press, New York, 1964) was seen to be singular in cases where the eigenvalues coincided (cases where the magnetic field is parallel or perpendicular to the direction of wave propagation, in the 1D case, $\hat{x}$). Brio and Wu proposed a renormalization procedure to handle this but their set of eigenvectors still contained a singularity at the "triple umbilic" point where the magnetic field is aligned to the direction of propagation and the Alfvén wave-speed coincided with the speed of sound. They applied a Roe-type upwind scheme but could construct the Roe-averaged Jacobian at the interface only for special case of $\gamma = 2$. For other values of γ, they used arithmetic averaging for the primitive variables. In the same study, the non-convexity of the MHD system was demonstrated. It has been shown that for case when the speed of sound is greater (lesser) than the Alfvén wave-speed, the slow (fast) characteristic field becomes degenerate when the transverse magnetic field goes through zero. This is the numerical manifestation of the non-isotropic wavespeeds seen in the previous section. In their numerical experiments, this non-convexity was seen in the form of the slow compound wave, which is seen in the implementation done here too, as described in the next chapter. The two coplanar 1D problems used by Brio and Wu have become benchmarks to test 1D MHD codes and are solved for in the current study.

Similar efforts on the 1D system have been made by Zachary and Collela [6] where they have applied a modification of the Engquist - Osher flux. Their system of eigenvectors is similar to that of Brio and Wu except that they have derived it from the equations written in terms of the primitive variable (with the inverse of density instead of density). The HLL class of approximate solvers have also been applied to the 1D system with excellent results and a complete discussion regarding the performance of these methods on the MHD system can be found in [34] and references therein. Roe and Balsara [13] have proposed a complete set of left and right eigenvectors which are well-defined at all points including the "triple umbilic". However the drawback of their eigen-system is that it has been derived from the 1D system written in terms of primitive variables. Thus, to use it in conservative schemes, they have to be appropriately pre-/post-multiplied with the Jacobians of transformations between primitive and conserved variable space. Cargo and Gallice [14] have proposed a method to find a Roe-averaged matrix for the interface for any value of γ. However, it has been demonstrated in [13] that the computed flux is insensitive to the choice of averaging and thus, most schemes use arithmetic averaging.

Attempts at extending 1D schemes to multi-dimensions have shown that a straightforward extension is not possible. One of the major obstacles is the necessity to ensure a divergence free magnetic field in the numerical solution. Neglecting this aspect may lead to non-physical solutions. It has been shown in [35] that for non-zero divergence of the magnetic field, the magnetic flux, momentum and energy are not conserved quantities since the momentum conservation, induction and energy conservation equations of the ideal MHD system, eq. (2.12), cannot be written in strict conservation form. Another non-physical effect of non-zero divergence is a non-zero component of the Lorentz force parallel to the magnetic field. Thus, in view of these inaccuracies, it is imperative that the solenoidal nature of the magnetic field be maintained at all time steps. While in 1D, this reduces to a simple condition of $B_x = constant$, which is satisfied by not including B_x in the evolution equations; in multi-dimensions, it is equivalent to zero total magnetic flux through the cell boundary edges/surfaces.

$$\nabla.\mathbf{B} = 0 \Rightarrow \sum_{faces} \mathbf{B_n}.ds = 0 \qquad (2.23)$$

Thus, unlike the 1D case, a jump is allowed in the normal component of the magnetic field as long as the above equation is satisfied. Presently, there are three different approaches being used to ensure this condition:

- *Projection Scheme*: A Poisson equation is solved which is used to subtract of the portion of the magnetic field with non-zero divergence. This method has been formulated in [35].

- *Constrained Transport / Central Difference* (CT/CD) using a staggered mesh: This method involves a discretization on a staggered grid for the magnetic field variables which are updated using Godunov fluxes. Zero divergence is obtained to the order of round-off errors. This method has been used in [7]

- *Eight-wave formulation*: This method has been suggested in [29] and applied in [3]. The multi-dimensional MHD system is modified to include source terms proportional to $\nabla.\mathbf{B}$. This leads to an eight-wave eigenstructure with an additional wave as the "divergence wave". The drawback is that the formulation is not strictly conservative and thus, inaccuracies may result in shock-capturing.

Multi-dimensional solvers based on these methods have been used to simulate many astrophysical problems like the interaction of the solar wind with the planetary magnetic field [3] and hypersonic blunt body computations [4].

Chapter 3
1D MHD System

The 1D system can be obtained from the ideal MHD system, eq. (2.12), by assuming that the gradients exist only along the x-direction. The resulting system can be written in conservative form as:

$$\mathbf{u}_t + \mathbf{f(u)}_x = 0 \tag{3.1}$$

where $\mathbf{u}$ is the conserved vector and $\mathbf{f(u)}$ is the flux vector.

$$\mathbf{u} = \begin{bmatrix} \rho \\ \rho u \\ \rho v \\ \rho w \\ B_y \\ B_z \\ E \end{bmatrix}, \; \mathbf{f(u)} = \begin{bmatrix} \rho u \\ \rho u^2 + P^* \\ \rho uv - B_y B_x \\ \rho uw - B_z B_x \\ uB_y - vB_x \\ uB_z - wB_x \\ (E + P^*)u - B_x(uB_x + vB_y + wB_z) \end{bmatrix} \tag{3.2}$$

In 1D, the zero divergence constraint results in the condition $B_x = constant$ which is satisfied by the above system.

3.1 The 1D MHD Eigenstructure

The above system, eq. (3.1), is hyperbolic in nature, with seven eigenvalues and a complete set of eigenvectors. It is not a strictly hyperbolic system since five out of seven eigenvalues can coincide. The wave structure of this system is given by the seven waves:

- Entropy wave with wave-speed $\lambda_e = u$
- two Alfvén waves with wavespeeds $\lambda_a^\pm = u \pm c_a$
- two fast magneto-sonic waves with wavespeeds $\lambda_f^\pm = u \pm c_f$
- two slow magneto-sonic waves with wavespeeds $\lambda_s^\pm = u \pm c_s$

where

$$c_a = B_x / \sqrt{\rho} \tag{3.3}$$

$$c_{f,s}^2 = \frac{1}{2}[\frac{\gamma p + \mathbf{B.B}}{\rho} \pm \sqrt{(\frac{\gamma p + \mathbf{B.B}}{\rho})^2 - \frac{4\gamma p B_x^2}{\rho^2}}] \tag{3.4}$$

as derived from eqs. (2.19) and (2.20) for propagation along the x-direction. Figure (3.1) illustrates these waves. These eigenvalues can coincide for two cases:
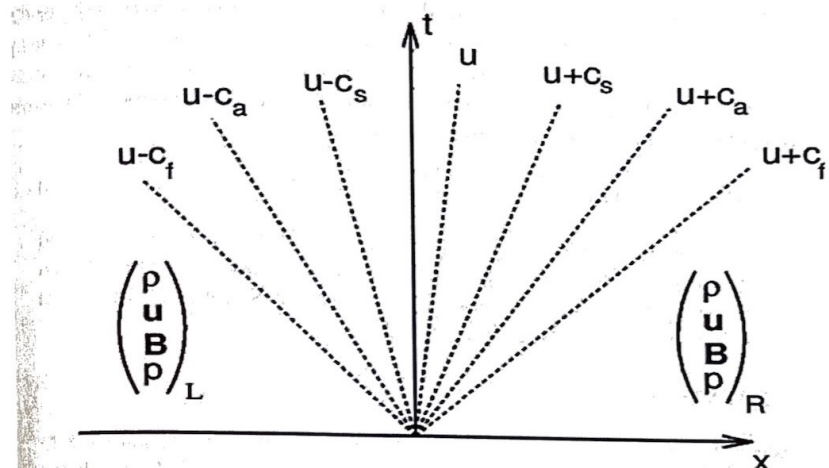
Figure 3.1: Waves in 1D

- $B_x = 0$ (Direction of propagation is perpendicular to the magnetic field): In this case, the Alfvén and slow wavespeeds coincide with the entropy wave since $c_a = c_s = 0$ and thus u is an eigenvalue with multiplicity 5. The problem becomes equivalent to a aerodynamic problem if the gas pressure is replaced with the full pressure. The fast magneto-sonic wave-speed is equivalent to the speed of sound.

- $B_y^2 + B_z^2 = 0$ (Direction of propagation is parallel to the magnetic field): In this case, $c_f^2 = max(a^2, c_a^2)$ and $c_s^2 = min(a^2, c_a^2)$ where a is the speed of sound ($a = \gamma p/\rho$). Thus, for $a^2 \neq c_a^2$, the eigenvalues $u \pm c_a$ are of multiplicities 2. Additionally, if $a^2 = c_a^2$, then the multiplicities of $u \pm c_a$ is 3. This point has been referred to as the "triple umbilic" in [13].

The eigenvectors for this system, proposed by Jeffrey and Tanuiti, were incomplete and became singular near these cases. Brio and Wu [5] used a renormalization process to ensure that their set of eigenvectors were well-defined at all points. Presently, two different eigen-structures exist for this system. One has been proposed by Roe and Balsara [13] and is derived from the governing equations written in terms of primitive variables. The other has been proposed by Ryu and Jones (*Numerical Magnetohydrodynamics in Astrophysics: Algorithm and Tests for One-Dimensional Flow*, Astrophysics Journal, 442 (1995), pp. 228 - 258) and is derived from the governing equations written in terms of the conserved variables. It has been reported [7] that though both yield the same result in 1D, the Ryu and Jones eigenstructure is unstable leading to negative pressures and densities in multi-dimensional problems. In the present study,

Roe and Balsara's eigenstructure is used. Near the cases where the eigenvalues coincide, as mentioned above, the normalization of the eigenvectors is the same as that used in [13]. These eigenvectors are derived from the governing equations written in terms of the primitive variables ($\mathbf{w} = [\rho, u, v, w, B_y, B_z, p]^T$). To use these in a scheme based on the conservative form, given by eq. (3.1), they need to be transformed as follows:

$$\mathbf{L_k} = \mathbf{l_k}\frac{\partial \mathbf{w}}{\partial \mathbf{u}}, \quad \mathbf{R_k} = \frac{\partial \mathbf{u}}{\partial \mathbf{w}}\mathbf{r_k}, \quad k = 1, ..., 7 \tag{3.5}$$

where $\partial \mathbf{w}/\partial \mathbf{u}$ and $\partial \mathbf{u}/\partial \mathbf{w}$ are the Jacobians of transformation between the conserved and primitive variable spaces [3, 7]. These matrix multiplications are carried out analytically and the final expressions are used in the code. Thus, a complete and well-defined set of orthonormal eigenvectors in the conserved variable space is obtained.

3.2 1D MHD Wave Structure

Although the Euler equations are underlying in the MHD system, the wave structure is substantially more complicated than that in gas-dynamics. The primary reason for this is the non-convexity of the MHD equations which leads to many non-evolutionary discontinuities (intermediate shocks over which more than one family of characteristics converge). These discontinuities are solutions of the MHD Rankine Hugoniot jump conditions [1] and their physical relevance has been debated over the last few decades and is still shrouded in controversy [10, 12, 21, 28]. Initially, all non-evolutionary shocks were rejected as physically irrelevant and admissible shocks were restricted to regular slow and fast shocks, across which only the slow and fast family of characteristics converged respectively. Both these shocks are compressive and across them, the magnetic field can change in magnitude only (the direction remaining the same). Additionally, the linearly degenerate rotational discontinuity (which changed the orientation of the magnetic field without changing its magnitude or affecting any of the flow variables) was believed to be responsible for any kind of rotation of the magnetic field. The primary argument against the existence of intermediate shocks were their acute sensitivity to non-planar perturbations in the magnetic field. Such shocks, like the compound waves observed in [5], exist only for the case when the end states of a Riemann problem are coplanar (having anti-parallel magnetic fields). These waves provide a mechanism for changing the sign of the transverse magnetic field. Although they are solutions of the planar MHD Rankine - Hugoniot jump conditions, they do not satisfy the non-planar jump conditions and thus, they are expected to degenerate when any non-planar wave impinges on them. Thus they were rejected as physically irrelevant, since in practical problems, the occurrence of perfectly coplanar conditions is improbable.

However, in recent times, such compound waves were observed in numerical computations starting with Brio and Wu's shock tube solution [5]. Additionally, an interplanetary intermediate shock was detected in the Voyager 1 data (Chao J.K., Lyu L.H., Wu B.H., Lazarus A.J.,

Chang T.S., *Observations of an intermediate shock in interplanetary space*, Journal of Geophysical Research, Vol. 98, 1993, pp. 17433 - 17450). These observations led to the debate over the relevance of evolutionary conditions, which were developed for convex, strictly hyperbolic system, to the MHD system.
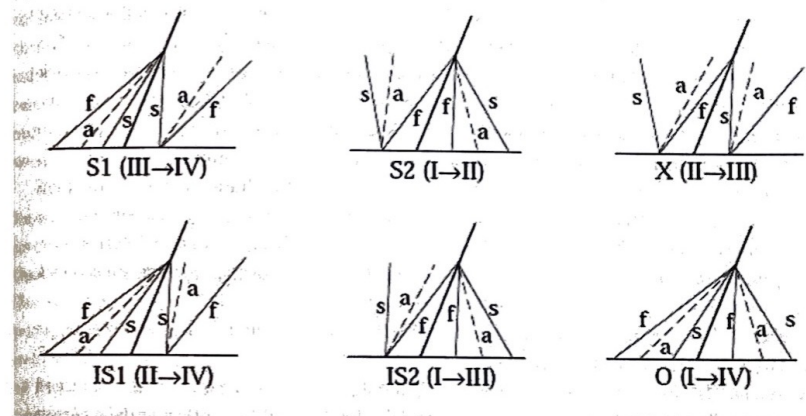

Figure 3.2: Admissible Shocks of the MHD Riemann problem [12]

The physical relevance of intermediate shocks was first studied in a series of papers by C.C. Wu [9, 10], by modeling the resistive MHD equations and demonstrating the formation, evolution and stability of intermediate shocks with converging Alfvén characteristics. Across the intermediate shock the sign of the tangential component of the magnetic field changed sign. In [10] and earlier works by Wu, it was demonstrated that these shocks could form due to steepening of continuous waves (such numerical experiments are reproduced in [20]) and thus should be considered physically relevant. The stability of the intermediate shock has been demonstrated through its interaction with an intermediate wave, carrying a non-planar flux [9]. According to the evolutionary theory, such an interaction should result in the immediate degeneration of the intermediate shock, which however did not occur in the numerical computations. The disintegration of the intermediate shock was found to be contingent on the boundary conditions and the dissipation present in the system. The initial conditions in [9] consisted of an intermediate shock with shock-frame velocities sub-fast, super-Alfvénic and super-slow upstream and sub-fast, sub-Alfvénic and sub-slow downstream. Thus, the converging characteristics on the upstream side included the slow and Alfvén families while downstream of the shock, all families of characteristics converged. Further, the initial condition contained an intermediate wave which caused a rotation in the magnetic field. Since intermediate waves

are convergent on the shock and cannot propagate ahead of it, the incoming flux of non-planar magnetic field component should cause the intermediate shock to disintegrate immediately, as dictated by the Rankine-Hugoniot jump conditions. However, it was observed that the intermediate wave was trapped inside the shock for a finite time, during which the non-planar flux reached a critical value. Disintegration occurred after this critical value was reached. It was also seen that disintegration could be avoided if the initial Alfvén wave had a fluctuating form or the dissipation was sufficient to damp the non-planar flux below the critical value. This demonstrated the existence of the neighboring solution to the initial coplanar intermediate shock having a rotation in the magnetic field. This "intermediate shock" - like structure, being non-coplanar does not satisfy the ideal MHD jump conditions but was a solution of the dissipative MHD. This led Wu [9, 10] to question the relevance of the ideal MHD equations, whose jump conditions precluded a class of possibly physically relevant intermediate shocks. Numerical simulations of the ideal MHD system inadvertently have a finite amount of dissipation built in, depending on the grid resolution and scheme used and thus, such non-coplanar intermediate shocks appear in the solution and lead to non-uniform convergence as discussed in subsequent sections.

Following these investigations, a systematic study of the wave structure in MHD was made by Myong and Roe [25, 26] using simplified model systems which preserved the hyperbolic singularities of the MHD system and had topologically similar solutions. These models contained waves corresponding to right-moving waves for the full MHD model for both planar/coplanar and non-planar cases. To address the limitations of the evolutionary conditions for shock admissibility, the viscosity admissibility condition was derived and applied to the planar/coplanar and non-planar model systems. This criteria admitted discontinuities which had a viscous profiles and were traveling wave solutions of the associated viscous equations. It is their contention that without the non-evolutionary discontinuities, the planar/coplanar Riemann problem cannot be solved for all initial conditions. However, with the inclusion of such waves, the planar/coplanar problem is well-posed and has an unique solution for all cases. The admissible discontinuities were found to be the regular slow/fast shocks (with only one family, slow/fast, converging across the shock), the over-compressive shock (across which all families of characteristics converge) and slow/fast compound waves (shock and rarefaction of the same family propagating together). Using these discontinuities and slow/fast rarefaction waves, any planar Riemann could by uniquely solved. For a non-planar problem, the solution is expected to contain (apart from the planar waves), Alfvén waves which rotate the magnetic field. The admissible non-planar discontinuities were found to be slow/fast intermediate shocks across which the Alfvén characteristics converged, in addition to the slow/fast characteristics. The relationship between the shock speed and the characteristic speeds are shown in Fig. (3.2) [12]. Borrowing the terminology in [12, 25, 26], $S1$ and $S2$ are the slow and fast regular shocks while X, $IS1$, $IS2$ and O are the intermediate shocks. Due to the extreme sensitivity of these intermediate shocks and compound waves in a non-planar setting, there occurrence is improbable and temporary. Thus, the conclusions from [12, 25, 26] indicate that the large-time solution is expected to contain only regular shocks (fast or slow) and broad Alfvén waves to change the direction of the magnetic field. The primary significance of these intermediate shocks is to explain the small-time behavior of the solution. By the viscous admissibility conditions, the existence of rotational discontinuities was rejected since they did not have corresponding traveling wave solution in a viscous setting. According to [25], the non-planar Riemann problem is not self-similar and the solution depends on the time scales involved. For very small times, the solution is expected to contain intermediate waves and structures like the compound waves. At intermediate times, the solution topology keeps changing as the non-evolutionary waves disintegrate into evolutionary ones. The rate of disintegration depends on the viscosity present in the system. At large times, only planar, evolutionary shocks are present and intermediate waves are replaced by Alfvén waves.

Inspite of these studies by Wu [9, 10] and Myong & Roe [25, 26] on the admissibility of intermediate waves, there still exists a school of thought who support the evolutionary theory and refute the existence of intermediate waves. It has been shown in [28] and reference therein, that the numerical results obtained in [5, 9, 10] and other such studies can be explained on the basis of the evolutionary theory without subscribing to the admissibility of intermediate waves. It was claimed in [25] that not all planar Riemann problems can be solved for using just evolutionary shocks and thus, non-evolutionary shocks are required to ensure the well-posedness of the solution. It has been subsequently refuted [28] on the grounds that initial conditions requiring such intermediate waves form a region of zero volume in the parameter space (thus reiterating the structural instability of intermediate waves to non-planar perturbation) and are physically irrelevant. Thus, on these grounds, these waves have been disregarded as acceptable solutions of the MHD system. Overall, questions regarding MHD wave structure and admissible discontinuities are yet to be resolved.

3.3 Model Systems

The model systems are simplified systems which retain the wave structure and singularities of the ideal MHD system. These systems have been used to study the wave structure of the ideal MHD system in [25, 26]. A rotationally degenerate 2×2 system has been presented in [25, 27] which provides a model to study the behavior of Alfvén waves. In [27], this system has been termed as a prototype of larger systems exhibiting rotational degeneracy, based on the correspondence between the wave behavior of the 2×2 system and the transverse part of the wave behavior of any rotationally degenerate system of hyperbolic conservation laws. Magnetohydrodynamics and isotropic elasticity are two such systems where this comparison applies. The system has a cubic flux function and is given by [25, 27]

$$\begin{bmatrix} u \\ v \end{bmatrix}_t + \begin{bmatrix} (u^2 + v^2)u \\ (u^2 + v^2)v \end{bmatrix}_x = 0 \tag{3.6}$$

The system is non-strictly hyperbolic, consisting of two characteristic directions (fast radial and slow angular modes) with eigenvalues as

$$\lambda_1 = 3(u^2 + v^2), \ \lambda_2 = (u^2 + v^2) \tag{3.7}$$

These eigenvalues coincide for $u = v = 0$. Away from this singularity, the fast radial mode is genuinely non-linear while the slow angular mode is linearly degenerate. The corresponding left and right eigenvectors are presented in [27]. The behavior of numerical schemes for this system and the associated complications have been studied in [27]. Solutions to Riemann problems are expected to contain two waves, one of each family. The slow angular mode results in a rotational discontinuity (the term "contact discontinuity" has been used in [27]) across which the solution vector rotates without changing its magnitude. The fast radial mode causes shocks and rarefactions across which the magnitude of the solution changes. This system faces a problem of non-uniqueness of solution for Riemann problems involving a rotation of π radians (see discussions in [27]) which is similar to the problems of non-uniqueness and debates regarding the admissibility of non-classical waves in the ideal MHD system (as discussed in this report and in [21]).

The representation of the ideal MHD equations using a 3×3 model system is based on the symmetric nature of the MHD waves around the fluid velocity. The simplified model, derived in [25], consists of the right-running waves of the ideal MHD system (with respect to the fluid motion) and is given as

$$\begin{bmatrix} u \\ v \\ w \end{bmatrix}_t + \begin{bmatrix} cu^2 + v^2 + w^2 \\ 2uv \\ 2uw \end{bmatrix}_x = 0 \tag{3.8}$$

The correspondence between the quantities of this system and the ideal MHD equations can be expressed as

$$c \equiv \gamma + 1, \ u \equiv (\frac{a}{c_a})^2 - 1, \ v \equiv \frac{B_y}{B_x}, \ w \equiv \frac{B_z}{B_x} \tag{3.9}$$

where $a = \sqrt{\gamma P/\rho}$ is the speed of sound. The details of the derivation are presented in [25]. The system is non-strictly hyperbolic admitting three waves (Alfvén, fast and slow) and the eigenvalues are

$$\lambda_a = 2u \ (\text{Alfven})$$
$$\lambda_{f,s} = (c+1)u \pm \sqrt{(c-1)^2u^2 + 4(v^2 + w^2)} \ (\text{Fast, Slow}) \tag{3.10}$$

always satisfying $\lambda_s \leq \lambda_a \leq \lambda_f$. One of the slow/fast wavespeeds vanish when $cu^2 = v^2 + w^2$ while the triple umbilic occurs at $u = v = w = 0$. The right and left eigenvectors for this system have been derived in [25] and the normalization required for the singularity at $u = v = w = 0$ has been outlined in [12]. For planar Riemann problems, the solutions to this system are expected to contain two waves (shock/rarefaction/compound wave) of each magnetosonic family (slow/fast). Since out-of-plane component of the state vector is identically zero ($w = 0$) for this class of

problems, the Alfvén mode is absent. The planar assumption also simplifies this system to yield a 2×2 model system [25], composed of the slow and fast characteristic fields. However, this planar system has not been used for numerical computations due to the lack of a suitable set of normalized eigenvectors. Solutions to non-planar Riemann problems are expected to contain, in addition to the planar slow/fast waves, a rotational wave of the Alfvén family. Based on the mathematical similarities between the 3×3 model system and the ideal MHD equations, the solutions of the two systems are expected to be topologically similar. As mentioned in the previous section, the admissible waves of the model systems have been derived in [25] and the results extended to the ideal MHD system [26] to yield a comprehensive description of the wave structure.

Thus, the 2×2 rotationally degenerate system provides a model field of the MHD system while 3×3 model system provides a model of the Alfvén characteristic right-running MHD waves. In the present study, these simplified systems are used to study the behavior of higher order WENO schemes and the necessity and efficacy of the monotonicity preserving limits on each characteristic field in MHD. Each of these systems (given by eqs. (3.6) and (3.8)) in the conservative formulation as given by eq. (3.1) are numerically solved as described in the next section. The behavior of the numerical schemes for the rotationally degenerate model system is studied to determine the necessity of using monotonicity preserving limits for the Alfvén mode. Further, the 3×3 model system is studied using various planar initial conditions to investigate the efficacy of MP limits for planar waves (shocks/rarefactions/compound waves). The initial conditions are obtained from the Riemann curves and Hugoniot loci presented in [25] such as to yield permutations of waves of different types and families. Additionally, non-planar initial conditions are used to study the behavior of the Alfvén mode and verify the conclusions drawn from the 2×2 rotationally degenerate system. Finally, the MP limits are applied to the ideal MHD equations and their performance assessed for various planar and non-planar Riemann problems.

3.4 Numerical Formulation

The semi-discrete form of eq. (3.1) can be written as

$$\frac{du_i}{dt} = \text{Res}(u_i); \ \text{Res}(u_i) = -\frac{1}{\Delta x}(F_{i+1/2} - F_{i-1/2}) \tag{3.11}$$

where i is the cell index and δx is the cell width. $F_{i-1/2}$ and $F_{i+1/2}$ are the numerical fluxes evaluated at the left and right interfaces of the ith cell. A characteristic-based scheme is used where the flux is reconstructed by decoupling along the characteristic directions. The eigenvalues, the left and right eigenvectors at the interface ($\lambda_{i+1/2}^k$, $L_{i+1/2}^k$ and $R_{i+1/2}^k$ respectively for $k = 1, ..., m$ where m is the number of characteristic directions of the system) used for decoupling, upwinding and re-coupling the fluxes are evaluated at an arithmetically averaged

state. The flux is evaluated as:

$$\mathbf{F}_{i+1/2} = \sum_{k=1}^{m} f_{i+1/2}^k \mathbf{R}_{i+1/2}^k \tag{3.12}$$

where $f_{i+1/2}^k$ is the component of the flux vector along the kth characteristic direction, evaluated numerically. For a scheme using a stencil S, characteristic flux at the interface is a function of those evaluated at cell centers lying in the stencil,

$$f_{i+1/2}^k = Rec(f_j^k; \ j \in S) \tag{3.13}$$

where Rec is the reconstruction procedure, dependent on the scheme used. In the present study, the Local Lax-Friedrich (LLF) and the Roe-Fixed (RF) formulations [17, 23] are used to evaluate the characteristic flux in an upwinded fashion. The behavior of both these formulations has been studied and it is observed that LLF yields more diffusive results compared to RF. However, the difference is negligible for fine grids and higher order schemes. The LLF formulation is given as

$$f_{i+1/2}^k = \tfrac{1}{2}[f_L^k + f_R^k + \alpha_{i+1/2}(u_R^k - u_L^k)]$$
$$\alpha_{i+1/2} = \chi max(|\lambda_i^k|, |\lambda_{i+1/2}^k|, |\lambda_{i+1}^k|) \tag{3.14}$$

where the subscripts L and R indicate a left- and right-biased evaluation of the flux respectively. The factor χ controls the amount of diffusion in the scheme and is typically between 1.0 to 1.3 [23]. The RF formulation is given as

$$f_{i+1/2}^k = f_L^k, \text{ if } \lambda_i^k, \lambda_{i+1/2}^k, \lambda_{i+1}^k > 0$$
$$= f_R^k, \text{ if } \lambda_i^k, \lambda_{i+1/2}^k, \lambda_{i+1}^k < 0$$
$$= \tfrac{1}{2}[f_L^k + f_R^k + \alpha_{i+1/2}(u_R^k - u_L^k)], \text{ otherwise} \tag{3.15}$$

Both these formulations require the evaluation of the left and right biased decoupled fluxes $f_{L,R}^k$ and states $u_{L,R}^k$ at the interface. The RF formulation uses the LLF as an entropy fix to the Roe's scheme by introducing extra dissipation and thus breaking up non-physical expansive shocks. Using the RF formulation is also computationally cheaper since reconstruction of the state vector is required only in cases where entropy fix is required. A more complete discussion on the comparison between RF and LLF formulations can be found in [23] and references therein. The semi-discrete equation, eq. (3.11), is advanced in time using the Runge-Kutta (RK) family of schemes [17]. The 1st order (Forward Euler), 2nd and 3rd order accurate Total Variation Diminishing (TVD) RK and 4th order RK schemes are used in the present study in conjunction with the high order WENO spatial discretization.

In the present study, computation of the decoupled fluxes $f_{L,R}^k$ are done using the ENO/WENO class of schemes. At the $(i+1/2)$th interface, the left biased decoupled flux f_L^k is computed using a stencil containing the ith cell while the right biased decoupled flux f_R^k is computed using

a stencil containing the $(i+1)$th cell. An r-th order ENO scheme chooses the smoothest stencil among r candidate stencils containing the upwind cell (i or $i+1$). The WENO schemes were introduced as an improvement over the ENO schemes [17, 18, 19] the selective procedure is replaced by taking a convex combination of all the candidate stencils, with weights dependent on the smoothness of the stencils. In smooth regions of the solution, these weights approach the optimum weights which yield a $(2r-1)$th order approximation, while near a discontinuity, the stencils which contain the discontinuity are given near-zero weights. Thus, an r-th order ENO scheme can be extended to give a $(2r-1)$th order WENO scheme. The left-biased decoupled flux at the $(i+1/2)$th interface, computed using a rth order ENO scheme centered on the ith cell is

$$f_L^k = f_j^k(f_{i-r+j+1}^k, f_{i-r+j+2}^k, ..., f_{i+j}^k) \text{ where } (f_j^k = \mathbf{L}_{i+1/2}^k.\mathbf{F}_j) \tag{3.16}$$

where

$$S_j = [i-r+j+1, i-r+j+2, ..., i+j] \tag{3.17}$$

is the locally smoothest stencil (based on the r-th divided difference) among r choices ($0 \le j \le r-1$).The same flux computed using a $(2r-1)$th order WENO scheme centered on the ith cell, can be formulated as:

$$f_L^k = \sum_{j=0}^{r-1} \omega_j^r f_j^k(f_{i-r+j+1}^k, f_{i-r+j+2}^k, ..., f_{i+j}^k) \tag{3.18}$$

Each of the r candidate stencils give an r-th order approximation $f_j^k(f_{i-r+j+1}^k, f_{i-r+j+2}^k, ..., f_{i+j}^k)$ and the coefficients for each point in the stencil can be found in [17] for various orders. The weights ω_j depend on the smoothness of the stencil and are constructed as:

$$\omega_j^r = \frac{\alpha_j^r}{\alpha_0^r + \alpha_1^r + ... + \alpha_{r-1}^r} \text{ where } \alpha_j^r = \frac{C_j^r}{(\epsilon + IS_j^r)^2} \tag{3.19}$$

C_j^r are optimum weights which result in a $(2r-1)$th order approximation while IS_j^r are smoothness indicators. A small number $\epsilon = 10^{-6}$ in added to the denominator to prevent division by zero. The values and expressions for the optimum weights C_j^r and the smoothness indicators IS_j^r for various orders r are given in [17, 19, 23]. The corresponding expressions, centered on the $(i+1)$th cell can be used to compute the right-biased decoupled flux f_R^k. A similar procedure is used to compute the left and right biased decoupled states $u_{L,R}^k$, wherever required.

3.5 Preliminary 1D Results

The schemes developed are applied to two planar Riemann problems as described in [5]. The first is Brio & Wu's shock tube which is an extension of the Sod's shock tube in hydrodynamics, with anti-parallel magnetic field components on either side of the initial discontinuity. The solution of this problem consists of a fast rarefaction, a slow shock and a contact discontinuity moving to the right and a fast rarefaction and a slow compound wave moving to the left. The second problem solved is the high Mach number problem which involves shocks moving

at approximately Mach 15. Since the magnetic field in this problem is perpendicular to the direction of propagation of waves (x-direction), it is equivalent to a hydrodynamic problem with the full pressure being equivalent to the gas pressure. Although these problems have no physical relevance, they have become benchmark problems in the numerical solution of 1D MHD and serve as validation cases. The initial conditions for these problems are as follows:
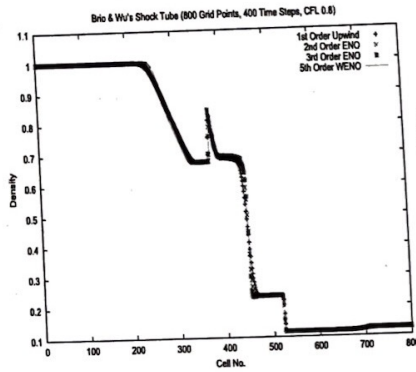

Figure 3.3: Density - case 1
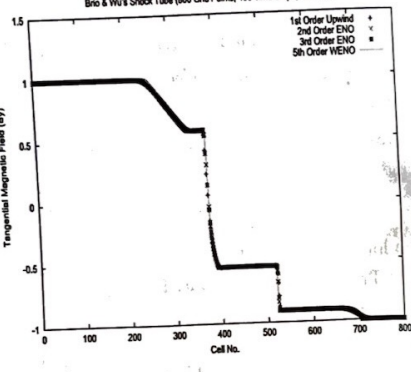
Figure 3.4: Tangential Magnetic Field - case 1
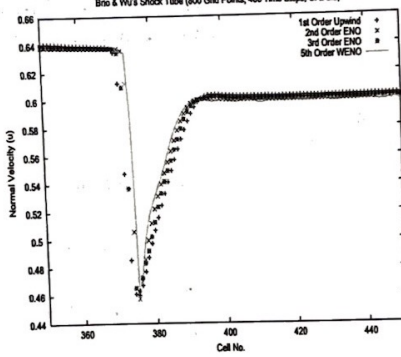
Figure 3.5: Normal Velocity (Magnified)
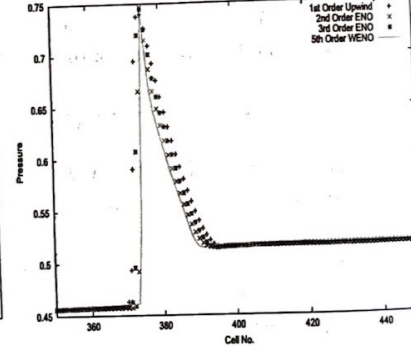
Figure 3.6: Pressure (Magnified)

Shock Tube (Case 1) : $\mathbf{w_L} = [1, \ 0, \ 0, \ 0, \ 1, \ 0, \ 1]$
$$\mathbf{w_R} = [0.125, \ 0, \ 0, \ 0, \ -1, \ 0, \ 0.1]$$
$$B_x = 0.75, \ \gamma = 2.0 \tag{3.20}$$
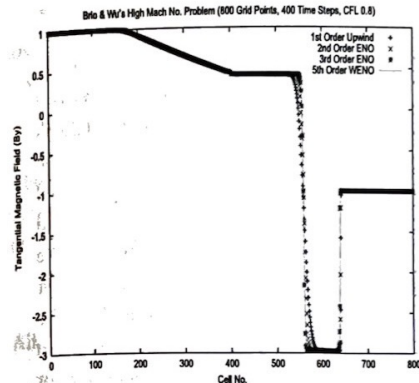
Figure 3.7: Tangential Magnetic Field - case 2
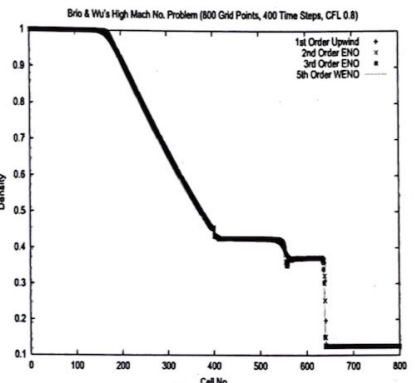
Figure 3.8: Density - case 2

High Mach No. (Case 2) : $\mathbf{w_L} = [1, \ 0, \ 0, \ 0, \ 1, \ 0, \ 1000]$,
$$\mathbf{w_R} = [0.125, \ 0, \ 0, \ 0, \ -1, \ 0, \ 0.1]$$
$$B_x = 0, \ \gamma = 2.0 \tag{3.21}$$

where $\mathbf{w} = [\rho, u, v, w, B_y, B_z, p]$ is the vector of primitive variables and the subscripts L and R indicate the left and right halves of the domain. The domain of computation is taken as $x \in [0, 1]$ with the initial discontinuity at $x = 0.5$. All computations are done on a grid containing 800 points and a CFL number of 0.8 for 400 time steps. In both the cases, the computed solutions are validated with those presented in literature.

Figs. (3.3) and (3.4) show the variation of density and tangential magnetic field respectively for the shock tube problem for all the schemes. In fig. (3.3), it can be seen from the density profiles that the resolution of the shocks and the contact discontinuity improves as the order of the scheme increases, with the 5th order WENO showing very little smearing. Figs. (3.5) and (3.6) show a magnified view of the compound wave in the solution, which consists of a shock attached to a rarefaction (this is a manifestation of the non-convex flux function). Figs. (3.7) and (3.8) show the variation of the log of pressure and density for the high Mach number problem. The Mach number corresponding to the right-moving shock wave is 15.5. Since this problem reduces to a standard hydrodynamical one with the full pressure being equivalent to the gas pressure and the fast magneto-sonic wave being equivalent to the speed of sound, the analytical solution can be found [5, 20]. Once again, it is observed that the smearing over the contact discontinuity reduces considerably as higher order schemes are used. In both the cases considered here, it is seen that the 5th order WENO scheme produces some oscillations near the rarefaction waves as well the contact discontinuities and these issues are addressed in the next section.

3.6 Monotonicity Preserving Limits

To improve the performance of the WENO schemes near discontinuities, the monotonicity preserving limits were suggested [23, 24] to prevent oscillatory behavior. High order WENO schemes have been reported to produce spurious oscillations, not only near discontinuities (shock waves and contact discontinuities) but also near rarefaction waves, in computations for the ideal MHD system [20, 23]. To address these problems, the MP limits have been suggested which prevent such spurious oscillations without degrading the accuracy near discontinuities and physically relevant extrema. These limits use the local curvature of the solution to determine the maximum and minimum bounds within which the reconstructed fluxes should lie to prevent spurious oscillations. MP limits have been applied to the MHD system in [23] and results have been presented for the Brio & Wu's problem which are encouraging. It has been seen in those studies that the MP limits are effective in alleviating the oscillatory behavior for WENO schemes. This limiting technique have also been applied to a number of one- and two-dimensional hydrodynamic problems and its efficacy has been shown for problems like shock-vortex interactions [23]. The construction of these limits and their use as outlined in [23, 24] is given below.

The measure of the curvature at the ith cell center is given as

$$d_i = f_{i+1} - 2f_i + f_{i-1} \qquad (3.22)$$

At the interface, the definition of the curvature can be obtained for the curvatures at the cell centers. A number of possibilities exists which differ in their allowance for an extremum to grow. The simplest, least restrictive measure is given as

$$d_{i+1/2}^{MM} = \text{minmod}(d_i, d_{i+1}) \qquad (3.23)$$

A more restrictive definition has been suggested by [24] where the space for the local extremum to grow is reduced when the ratio between adjacent cell centered curvatures exceed 4 or falls below 1/4. It is given as

$$d_{i+1/2}^{M4} = \text{minmod}(4d_i - d_{i+1}, 4d_{i+1} - d_i, d_i, d_{i+1}) \qquad (3.24)$$

The range [1/4, 4] has been determined heuristically and it has been shown that the resulting schemes are not overly dependent on this choice. It has been argued [23] that the spurious oscillations occurring in ideal MHD can be spread over upto four cell centers and thus the above curvature measures, which admit extrema spread over more than two cells, may not succeed in alleviating these. A curvature measure which admits extrema having a larger support base has been suggested in [23]:

$$d_{i+1/2}^{M4X} = \text{minmod}(4d_i - d_{i+1}, 4d_{i+1} - d_i, d_i, d_{i+1}, d_{i-1}, d_{i+2}) \qquad (3.25)$$

Both these curvature measures are used in the present study and it is seen that $d_{i+1/2}^{M4X}$ performs better for all classes of problems, especially for problems involving the 3×3 model system.

The upper and lower limits, within which the reconstructed values are required to lie, are obtained using the measure of the curvature at the interface [24, 23]. For the left-biased computations, the left-sided upper limit at the $(i + 1/2)$th interface is given as

$$f_{i+1/2}^{UL} = f_i + \phi(f_i - f_{i-1}) \qquad (3.26)$$

The maximum CFL number that can be used depends on the value of ϕ as $1/(1 + \phi)$. In the present study, ϕ is taken as 2.0, thus restricting the CFL number to below 0.33. The median at the interface is defined as

$$f_{i+1/2}^{MD} = \frac{1}{2}(f_i + f_{i+1}) - \frac{1}{2}d_{i+1/2}^{MD} \qquad (3.27)$$

Allowing for a large curvature, the left-sided value of the solution at the interface is given as

$$f_{i+1/2}^{LC} = f_i + \frac{1}{2}(f_i - f_{i-1}) + \frac{\beta}{3}d_{i-1/2}^{LC} \qquad (3.28)$$

It has been commented in [23] that the resulting schemes are not sensitive to the value of the parameter β which determines the allowance for an extremum to develop by using a large value of the curvature. This is verified in the present study and it is seen that the solutions do not differ by much for $\beta = 0.5$, $\beta = 2$ and $\beta = 4$. This property alleviates the disadvantage of tuning an additional parameter while using the schemes. For the curvature measure, $d_{i+1/2}^{MD} = d_{i+1/2}^{LC} = d_{i+1/2}^{M4}$ was taken in [24] while $d_{i+1/2}^{MD} = d_{i+1/2}^{LC} = d_{i+1/2}^{M4X}$ has been used in [23]. The latter is used in our computations since it has been seen to be more suited to the ideal MHD system. Based on these values, the maximum and minimum values within which the reconstructed values should lie, can be found as

$$f_{i+1/2}^{L,min} = \max[\min(f_i, f_{i+1}, f_{i+1/2}^{MD}), \min(f_i, f_{i+1/2}^{UL}, f_{i+1/2}^{LC})] \qquad (3.29)$$
$$f_{i+1/2}^{L,max} = \min[\max(f_i, f_{i+1}, f_{i+1/2}^{MD}), \max(f_i, f_{i+1/2}^{UL}, f_{i+1/2}^{LC})] \qquad (3.30)$$

The MP value for the left-biased reconstructed flux is obtained as

$$f_{i+1/2}^{L,MP} = \text{median}(f_{i+1/2}^L, f_{i+1/2}^{L,min}, f_{i+1/2}^{L,max}) \qquad (3.31)$$

where the median function is given as
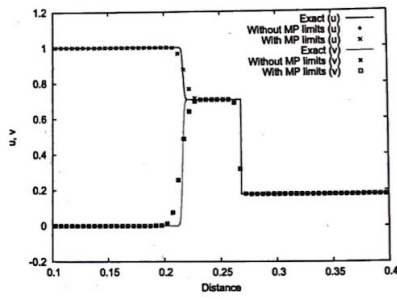
$$\text{median}(x, y, z) = x + \text{minmod}(y - x, z - x) \qquad (3.32)$$

The MP value for the right-biased reconstructed flux can be obtained similarly. This treatment is applied to the decoupled fluxes (and the state decoupled states, wherever required) along the characteristic directions.
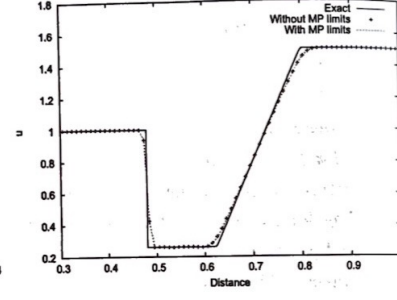
3.7 Results - Monotonicity Preserving Limits

The numerical scheme outlined above are applied to a number of 1D Riemann problems for the three systems considered in this study. A systematic study is made of the behavior of
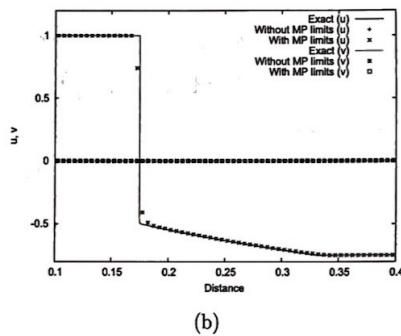
the WENO schemes, with and without the MP limits applied to the appropriate characteristic fields. In each of the cases, the "exact" solution is computed by using a first order accurate scheme on a grid with 80,000 points. For the rotationally degenerate system, the problems chosen are same as those used in [27]. The 3×3 model system is used to study the efficacy of MP limits over waves of various types (shock/rarefaction/compound) and families (slow/fast). Two non-planar problems are also used to investigate the necessity of MP limits on the Alfvén mode. For the 1D MHD system, the Riemann problems solved in section (3.5) are solved. In addition, two non-planar problems, which are modifications of the Brio & Wu's shock tube problem are solved to study the behavior of the Alfvén mode.


(a)

(a)

(b)
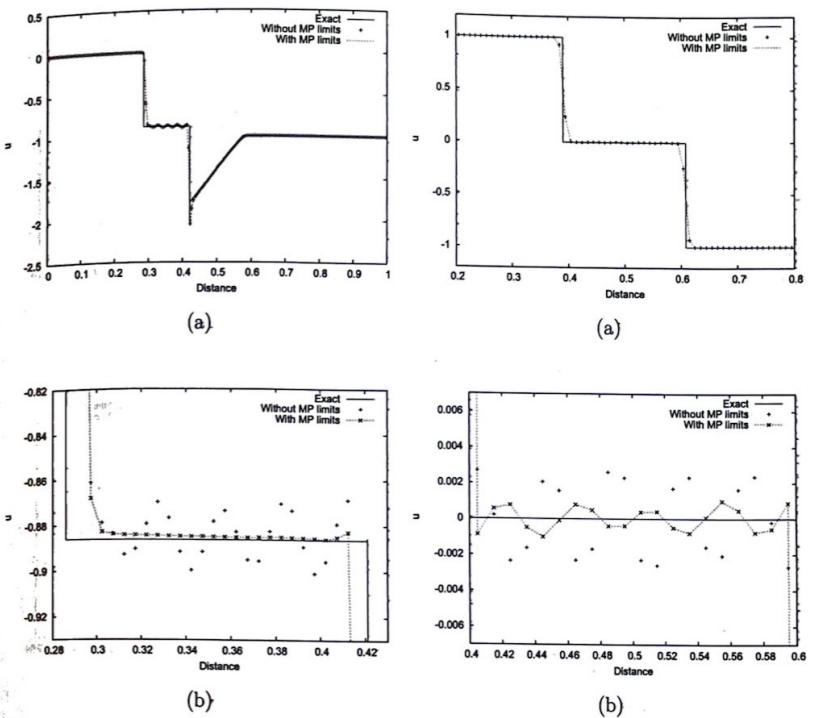
(b)

Figure 3.9: (a) Case 1 and (b) Case 2

Figure 3.10: (a) S1R2 (b) Magnified view

(a)

(a)

(b)

(b)

Figure 3.11: (a) S1C2 (b) Magnified view

Figure 3.12: (a) S1S2 (b) Magnified view

### 3.7.1 2×2 Rotationally Degenerate System
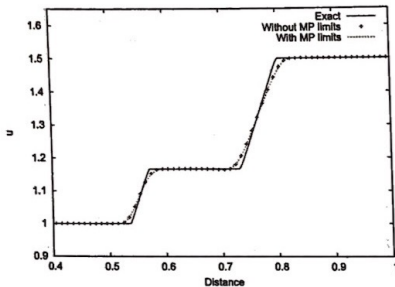
The numerical examples solved here are drawn from [27] where a class of Riemann problems have been solved using a Godunov-type method and the Random Choice Method. The initial conditions are given by ($0 \leq x \leq 1$):

$$\{u, v\}(x, t = 0) = \begin{cases} \{1, 0\} & \text{if } x \leq 0.05 \\ \{r\cos\theta, r\sin\theta\} & \text{if } x > 0.05 \end{cases} \tag{3.33}$$
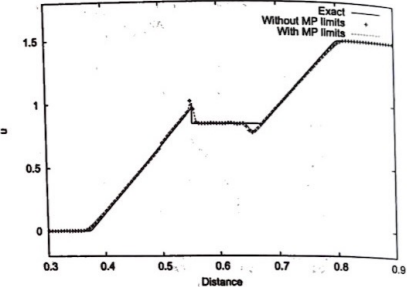
$$\text{Case 1}: \ r = 0.25, \ \theta = \pi/4$$
$$\text{Case 2}: \ r = 0.75, \ \theta = \pi$$
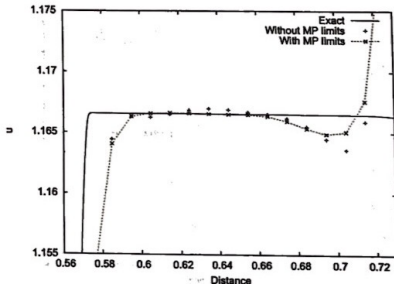
Computations are carried out on a grid of 200 points using three different orders of WENO scheme (5th, 7th and 9th) with and without MP limits and the solutions are compared with the
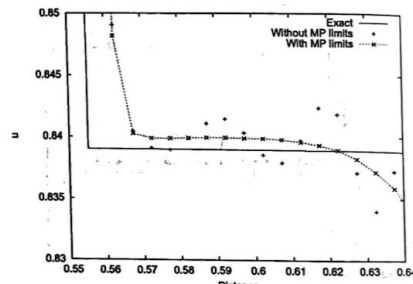
(a)

(b)
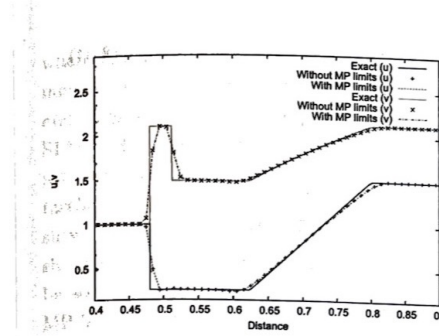
Figure 3.13: (a) R1R2 (b) Magnified view

(a)
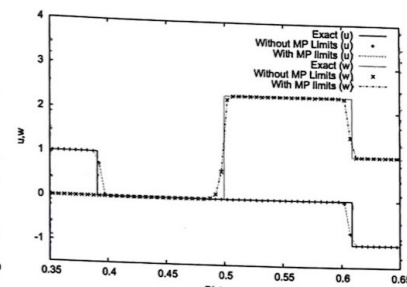
(b)

Figure 3.14: (a) C1R2 (b) Magnified view

(a)

(b)

Figure 3.15: (a) S1AR2 (b) Magnified view

(a)

(b)

Figure 3.16: (a) S1AS2 (b) Magnified view

exact solution. Figure (3.9) shows the variations of u and v for cases 1 and 2 using 9th order WENO scheme on a 200-point grid. The solution of case 1 consists of a slow rotational discontinuity across with the vector $[u\ v]^T$ rotates by $\pi/4$ radians without a change in magnitude and a fast shock across which the magnitude changes (decreases) without any rotation. The solution of case 2 consists of a compound wave of the slow family (shock attached to a rarefaction) This is one of the two admissible solutions for this particular initial condition, the other being a slow π radians rotational discontinuity and a fast shock (see [27] for a complete discussion on issues of non-uniqueness). It can be seen from the figure that oscillations are absent for orders as high as 9th order WENO and the solutions computed with and without MP limits coincide. Thus, it can be inferred from these observations that rotationally degenerate systems do not encounter problems of spurious oscillations when higher order spatial reconstruction is applied to them. Since this system is representative of the Alfvén wave-mode in ideal MHD, these observations indicate that the MP limiting treatment may not be required for the Alfvén mode on the ideal

MHD system and this is verified using non-planar Riemann problems in the next two sections.

3.7.2 3 × 3 Model System

Based on the observations from the 2×2 rotationally degenerate system, the 3×3 non-planar system is solved with MP limits applied to two of the three characteristic fields (slow and fast). Initially, five planar Riemann problems are solved, with the aim to study the behavior of MP limits across different classes of waves (shocks, rarefactions and compound waves). These problems contain two waves - one each of the slow and fast families. The initial conditions for these problems are obtained from the Riemann curves and Hugoniot loci for the model system (Fig. (7) in [25]) to yield different combinations of shocks, rarefactions and compound waves. The initial conditions for these problems are given by ($0 \le x \le 1$)

$$\{u, v, w\}(x, t = 0) = \{u, v, w\}_L \text{ if } x \le 0.5$$

$$\{u, v, w\}_R \text{ if } x > 0.5 \qquad (3.34)$$

S1R2 : $\{u,v,w\}_L = \{1,1,0\}$, $\{u,v,w\}_R = \{1.5,3,0\}$

S1S2 : $\{u,v,w\}_L = \{1,1,0\}$, $\{u,v,w\}_R = \{-1,1,0\}$

R1R2 : $\{u,v,w\}_L = \{1,1,0\}$, $\{u,v,w\}_R = \{1.5,0.5,0\}$

C1R2 : $\{u,v,w\}_L = \{0,2,0\}$, $\{u,v,w\}_R = \{1.5,1,0\}$

S1C2 : $\{u,v,w\}_L = \{0,2,0\}$, $\{u,v,w\}_R = \{-1,-3,0\}$

(C1 → Slow Compound Wave, C2 → Fast Compound Wave)

(S1 → Slow Shock, S2 → Fast Shock)

(R1 → Slow Rarefaction, R2 → Fast Rarefaction)

Computations are performed with $c = 3$ and a CFL number of 0.2 (the MP limits restrict the CFL to less than 0.33 for $\phi = 2.0$). Figure (3.10) shows the variation of u for S1R2 using 7th order WENO on a 100-point grid while figure (3.11) shows the variation of u for S1C2 using 9th order WENO on a 200-point grid. In both these cases, it is seen from the magnified views that the oscillations occur in the region between the two waves (the slow shock and the fast rarefaction in the former; the slow shock and the fast compound wave in the latter) and the MP limits are quite effective in damping these oscillations. The same conclusions can be drawn from observing S1S2 as shown in figure (3.12) which shows the variation of u for 9th order WENO on a 100-point grid. Figure (3.13) shows the variation of u for R1R2 for 7th order WENO on a 100-point grid. Oscillations are negligible in this case and are damped out with MP limits. For C1R2, shown in figure (3.14), there are small oscillations which are damped out with the MP limits. However, there is a deviation at the foot of the rarefaction which the MP limits are unable to remove. The deviation has a large support base and thus, it is perhaps misinterpreted by the MP limiting technique as a genuine extremum. Overall, it can be concluded from these results that the the magnetosonic modes are susceptible to spurious oscillations when subjected to higher-order schemes which can be improved upon by the MP limits.

As a verification of the conclusion that the Alfvén mode does not require MP-limits, two non-planar modifications of the previous problems are considered. Since the previous problems are planar with $w = 0$ throughout the domain, the Alfvén mode is absent. The modification involved a 45° and 90° twist to the vector $[v\ w]^T$ in the initial conditions for the right half of the domain (the vector $[v\ w]^T$ corresponds to the transverse magnetic field $[B_y\ B_z]^T$ in ideal MHD). In addition to the waves seen in the previous set of problems, these non-planar problems yield a rotational discontinuity across which v and w change while u remains constant. The initial conditions for the two non-planar problems considered here are given as:

S1AR2 : $\{u,v,w\}_L = \{1,1,0\}$, $\{u,v,w\}_R = \{1.5,2.12,2.12\}$
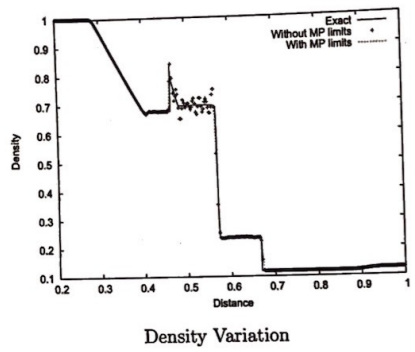
S1AS2 : $\{u,v,w\}_L = \{1,1,0\}$, $\{u,v,w\}_R = \{-1,0,1\}$

32

where A denotes a rotational discontinuity. Computations are performed for the same CFL number as before. The problems are solved with MP limits on the magnetosonic modes only and on all modes and the results compared. Figure (3.15) shows the variations of u and v for S1AR2. The initial conditions are a modification of the S1R2 case considered earlier involving a 45° rotation of $[v\ w]^T$ across the initial discontinuity. Apart from the slow shock and the fast rarefaction, there is a rotational discontinuity which is visible in the variation of v. The figure shows the computations for 9th order WENO scheme on a 100-point grid. The magnified view shows the variation of v between the fast rarefaction and the rotational discontinuity. It can be seen from the figure that there is a good agreement between the solution computed with MP limits on the magnetosonic modes and that computed with MP limits on all modes. The same conclusion can be drawn from S1AS2 as shown in figure (3.16). The initial conditions are a modification of the S1S2 case involving a 90° rotation of $[v\ w]^T$. The variation of u and w is shown for 9th order WENO scheme on a 100-point grid and the solution consists of a slow shock, a rotational discontinuity and a fast shock. The magnified view shows the variation of w between the fast shock and the rotational discontinuity. It is seen from both these examples that the solutions obtained using MP limits on all modes does not differ significantly with those not using MP limits on the Alfvén mode. Thus, in addition to the observations from the rotationally degenerate system in the previous section, it is confirmed here that the Alfvén mode does not require any limiting treatment.
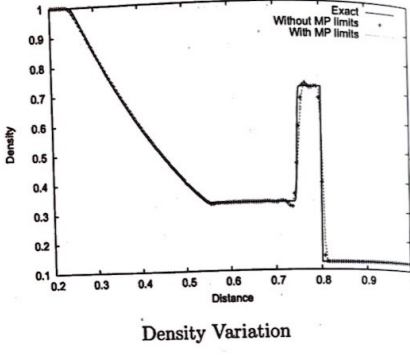
3.7.3 1D Ideal MHD

The 1D MHD system comprises of seven characteristic directions, two each of slow, Alfvén and fast modes (left and right running), and an entropy wave. The results from the model systems indicate that the Alfvén mode does not require the MP limiting techniques, while the slow and fast magnetosonic modes require them to damp out spurious oscillations. The entropy wave has no equivalent in the model systems and thus, the necessity of MP limits on this mode is assessed on the MHD system itself. It is seen that the entropy mode causes some oscillations and thus, MP limits are also used on this mode.
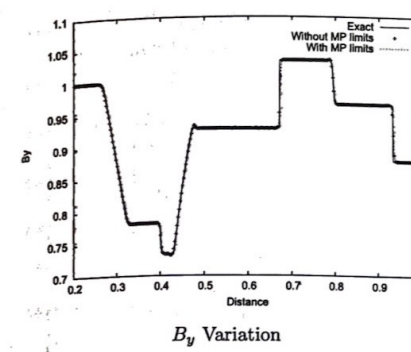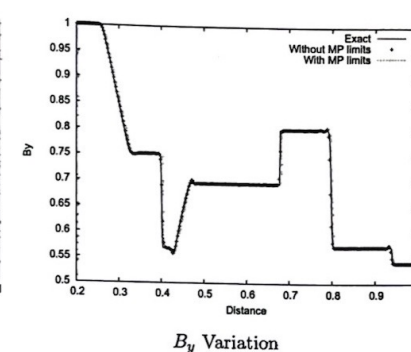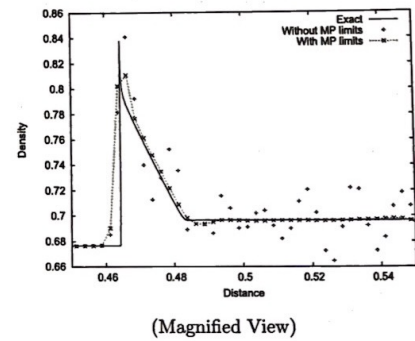
The two planar Riemann problems solved in section (3.5), given by eqs. (3.20) and (3.21), are solved using high order WENO schemes with and without MP limits on the magnetosonic and entropy modes. Computations are done with a CFL number of 0.3. Figure (3.17) shows the density variation of the Brio & Wu's shock tube on 400 grid points using 9th order WENO scheme with and without MP limits applied to the magnetosonic and entropy fields. It can be seen that without the MP limits, there is a considerable amount of oscillations downstream of the left-moving slow compound wave. These oscillations are effectively damped out using the MP limits and this can be seen more clearly in the magnified view. Similarly, figure (3.18) shows the density variation for the High Mach No. problem using 9th order WENO on a 200-point grid. In both the cases, it can be seen that the MP limits are very effective in damping out the oscillations, though it may increase the diffusion in the solution (see the magnified views of

33
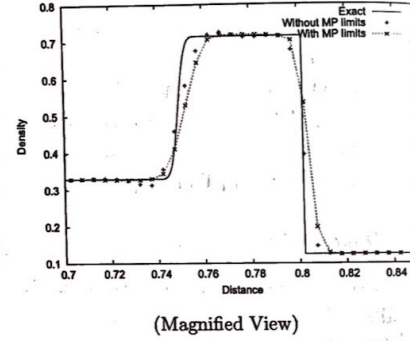
Density Variation

Density Variation

(Magnified View)

(Magnified View)

Figure 3.17: Brio & Wu's Shock Tube

Figure 3.18: High Mach No. problem

B_y Variation

B_y Variation

(Magnified View)

(Magnified View)

Figure 3.19: Non-Planar ($\theta = 0.5$ radians)

Figure 3.20: Non-Planar ($\theta = 1.0$ radians)

High Mach no. problem).
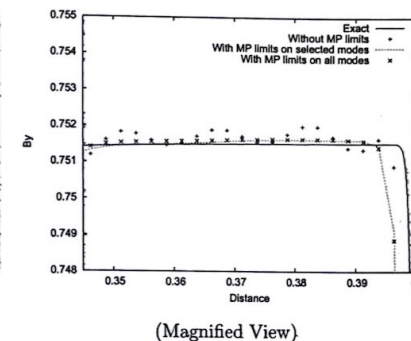
To study the behavior of the Alfvén mode, two non-planar modifications of the Brio & Wu's shock tube problems are considered. These problems are similar to the problems studied in [21] where issues regarding pseudo-convergence for a certain class of problems has been discussed (see next section). The initial conditions are given as:

$$\text{Non} - \text{Planar}: \quad \mathbf{w_L} = [1, \ 0, \ 0, \ 0, \ 1, \ 0, \ 1]$$
$$\mathbf{w_R} = [0.125, \ 0, \ 0, \ 0, \ cos\theta, \ sin\theta, \ 0.1]$$
$$B_x = 0.75, \ \gamma = 2 \tag{3.35}$$

To avoid the pseudo-convergence issues as discussed in the next section, the angles of rotation of the transverse magnetic fields are taken as $\theta = 0.5$ and $\theta = 1.0$ radians, away from the controversial region around $\theta = \pi$ radians. Apart from the waves seen in planar problems, the solutions to these problems contain a rotational discontinuity across which only the transverse

magnetic field changes. Figure (3.19) shows the variation of B_y for $\theta = 0.5$ radians while the magnified view shows the variation of density in the region between the left-running slow rarefaction and the right-running contact discontinuity. Figure (3.20) shows B_y for $\theta = 1.0$ radian and the magnified view of the region ahead of the left-running rotational discontinuity. While the oscillations occurring are damped effectively by the MP limits, there is a good agreement between the solution obtained by using MP limits on all modes and that obtained by using the limits on the magnetosonic and entropy modes.

Thus, the conclusions drawn from the 3×3 model system are seen to extend to the ideal MHD system. Table (3.1) compares the CPU time required for solutions involving MP limits on all characteristic fields and those involving MP limits of the magnetosonic and entropy fields with those not using MP limits. The computations are carried out on an SGI Altix 350 machine (1.5 GHz, Titanium twin-processor, compiled using -O3). While the usage of the MP limits entails a considerable increase in the computational cost, it can be seen that there is a

substantial decrease in the computational cost with selective use of MP limits and this decrease is amplified for finer grids. It is expected that the savings in computational cost will be larger for multi-dimensional problems.

Cases	5-A	5-S	5-N	7-A	7-S	7-N	9-A	9-S	9-N
Case 1									
400 Points	1449	1005	387	1652	1068	412	1702	1162	479
800 Points	6864	4497	1447	7416	4680	1692	7787	5008	2063
Case 2									
200 Points	314	238	77	324	252	91	352	274	131
400 Points	1345	1014	326	1399	1061	398	1517	1150	577

Table 3.1: 1D MHD: CPU time (seconds) comparisons - MP limits applied to selected modes vs. all modes (5,7,9 - Order of WENO scheme; A - All modes, S - Selected modes, N - No MP Limits)

3.8 Non - Uniform Convergence

Due to the controversies persisting regarding the wave structure in ideal MHD (discussed in section 3.2), a class of Riemann problems have been defined as non-unique with two possible solutions. This category consists of problems with co-planar end states and can have two solutions depending on the admissibility of intermediate waves and rotational discontinuities. Borrowing the terminology from [21, 22], the problem has an r-solution which contains regular waves (slow and fast shocks/rarefactions) and also a c-solution, which contains intermediate waves (like compound waves). In the r-solution, a sign change in the transverse component of the magnetic field is achieved by the rotational discontinuity. Figure (3.21) [21] illustrates with an example of a coplanar Riemann problem, similar to the Brio & Wu's shock tube [5], but with the initial data varying slightly. The r-solution consists of a fast rarefaction, a rotational discontinuity and slow shock propagating to the left and fast rarefaction, a slow shock and a contact discontinuity propagating to the right. The rotational discontinuity does not show up on the density plot since it only changes the orientation of (flips the sign of) the transverse magnetic field. The c-solution is similar to the r-solution except that the rotational discontinuity and the slow shock propagating to the left are replaced by a slow compound wave. This is the solution that has been obtained through all numerical schemes in literature. The only exceptions are methods which use the exact solution of the Riemann problem (eg: the Random Choice Method, see references in [11]) and these yield the r-solution.

For non-coplanar initial conditions, the MHD Riemann problem is unique and has a regular solution consisting of evolutionary waves. The compound wave satisfies the Rankine-Hugoniot jump conditions for only the coplanar case and does not exist for other angles of rotation. However it is seen that that for near-coplanar initial conditions, a sort of non-uniform convergence occurs. This behavior was studied in [21] for a range of second order schemes and for higher
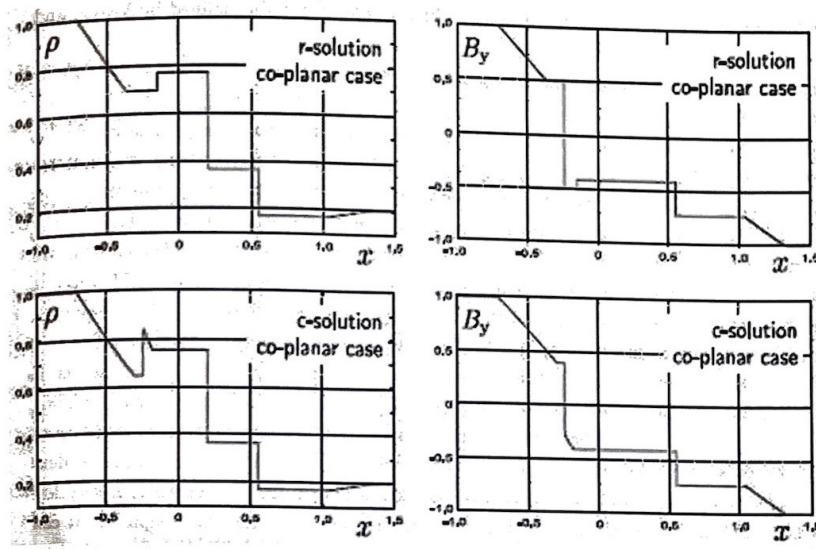

Figure 3.21: Possible Solutions of the coplanar Riemann problem [21]

order WENO schemes in [22]. For initial conditions that are slightly non-planar, it is seen that for low grid resolutions, the structure contains a compound-wave-like structure which causes a rotation in the magnetic field. However, this solution is *incorrect* since this kind of discontinuity violates the jump conditions. This behavior is studied in the 1D algorithms developed and similar behavior is observed for spatial orders going up to 7th order (ENO reconstruction). As the grid is progressively refined, the solution approaches the r-solution which is the correct solution by evolutionary arguments.

For the present investigation, non-planar modifications of the Brio & Wu's shock tube problem, as mentioned in the previous section, are used, but with different rotation angles. The initial conditions are given by eq. (3.35). For $\theta = \pi$ radians, this reduces to the coplanar Brio & Wu's problem. To study the non-uniform convergence behavior, a slightly non-planar orientation is chosen with $\theta = 3.0$ radians. Figure (3.22) and (3.23) show the density and magnetic field variations for computations using 800 and 20,000 points. All computations are performed using 5th order WENO reconstruction and 3rd order TVD time-stepping. The qualitative differences in the solution for $0.3 < x$ (*Length*) < 0.5 are obvious. While in the computations with 800 points, there is a slow compound-wave-like structure, the solutions for 20,000 points show a rotational discontinuity and a slow shock. It should be noted that even at 20,000 grid points, the resolution of the rotational discontinuity is imperfect. Thus, even slight

dissipation is enough to destroy its structure, which is why it was disqualified by Myong and Roe's viscosity admissibility criteria.

Figure (3.24) shows the breaking-up of the compound-wave-like structure as the grid is refined from 800 points to 20,000 points. As the grid is refined, the magnetic field variation approaches that of a rotational discontinuity while the density variation approaches that of a slow shock (ideally, it should not change across the rotational discontinuity, but even at 20,000 points, it fluctuates slightly). Figure (3.25) shows the solutions at different grid resolutions in the B_x-B_y plane. A radial curve represents a slow/fast shock or rarefaction wave changing the magnitude of the transverse magnetic field without changing its direction, while a circular arc depicts a rotational discontinuity, changing only the direction of the transverse field, without changing its magnitude. It can be seen that as the grid resolution is refined, the compound-wave-like structure breaks up and approaches a rotational discontinuity and a slow shock.

Although the coarse grid solution is an incorrect solution of the ideal MHD equations, it can be explained by the theories developed by Wu [10] and Myong & Roe [12] by considering the fact that the numerical schemes do not solve the ideal MHD equations but a modified set of equations, where the dissipation present in the system is a non-quantifiable amount, dependent on the scheme used. It was observed in [22] that use of higher order schemes with very low dissipations alleviated this problem slightly. Accounting for the numerical dissipation, it can be explained that the compound-wave-like structures are the intermediate waves studied by Wu, which are stable for slightly non-planar data and disintegrate as non-planarity increases or viscosity decreases. Additionally, using a time scale transformation as described in [22], the zero viscosity solution can be interpreted as the large time solution of the Riemann problem. Thus, using Myong & Roe's [25] description of non-linear evolution of waves and loss of self-similarity of the solution, the coarse grid solution can be said to represent the short time scales where the viscosity has not yet begun to act. Thus, intermediate waves are present in the solution. However, at large times (finer grids) these disintegrate into regular shocks and rarefactions as predicted in [25, 26]. Thus, considering the associated viscous equations, the theory developed in [9, 10, 25, 26] can be connected to the numerical results presented in this section and the problem of non-uniform convergence.

However, the fact still remains that these solutions, though explicable in the resistive MHD setting, are incorrect for the equations of ideal MHD, and therefore, one must aim to construct numerical schemes which will hasten the disintegration of the extraneous waves. Use of very high order schemes failed to resolve this problem [22] and helped only to bring down the threshold value of mesh refinement for which the solution approached the evolutionary one. Another method, suggested in literature, is adaptive mesh refinement around regions where the magnetic field undergoes a near-π rotation and where such waves are likely to occur.


(a) 800 Grid points
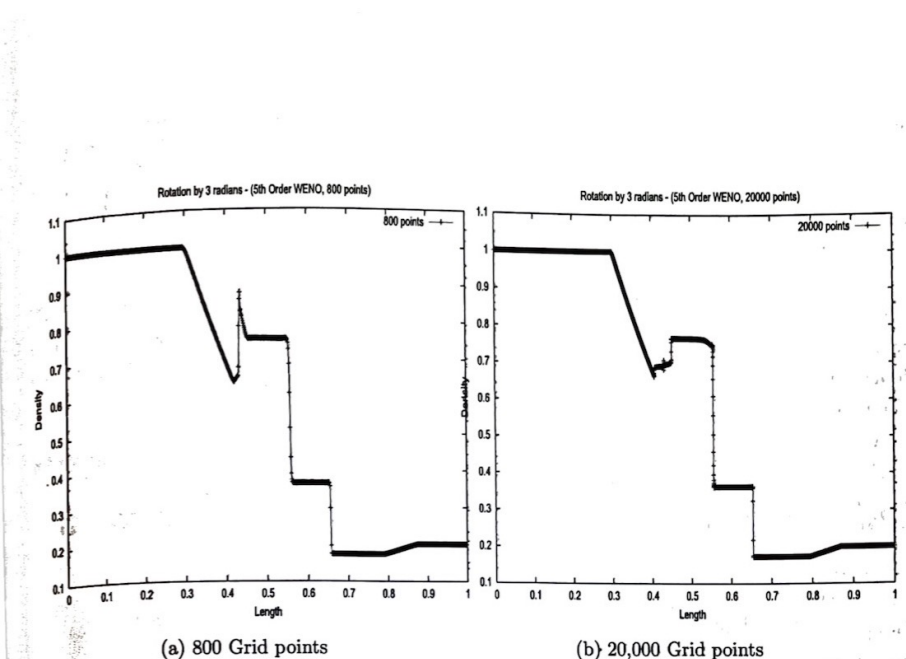
(b) 20,000 Grid points

Figure 3.22: Density Variation (800 and 20000 grid points)

(a) 800 Grid points
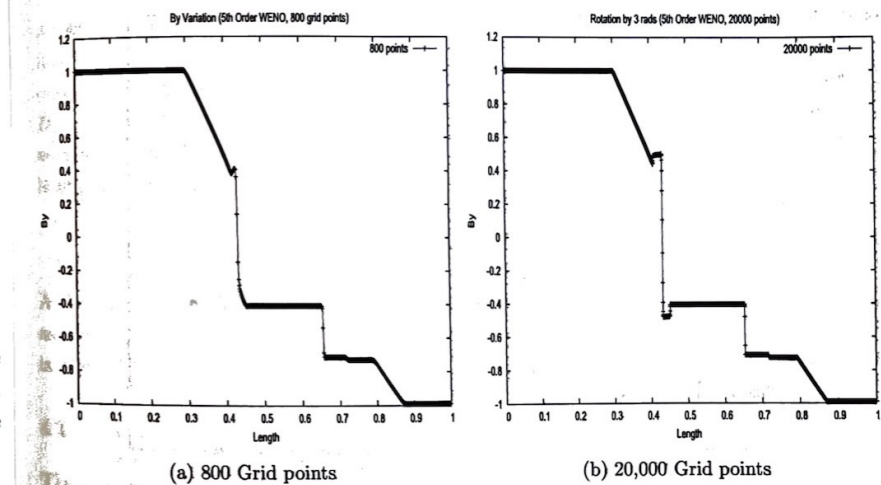
(b) 20,000 Grid points

Figure 3.23: B_y Variation (800 and 20000 grid points)

(a) B_y
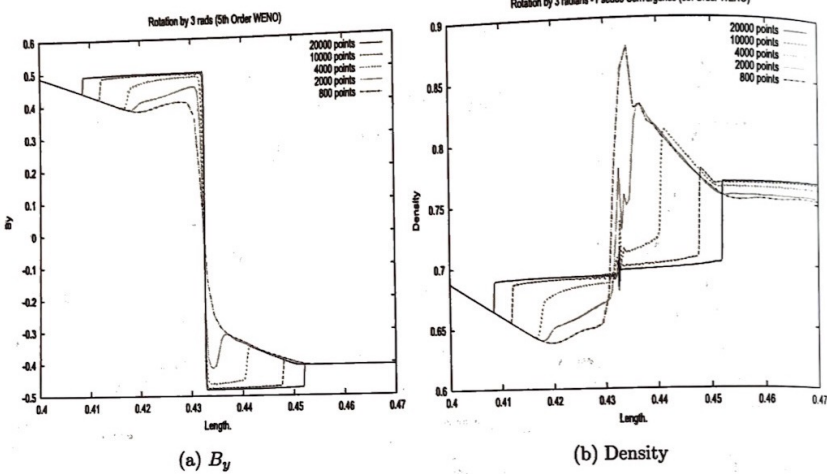
(b) Density

Figure 3.24: Break-up of the compound wave - density and B_y
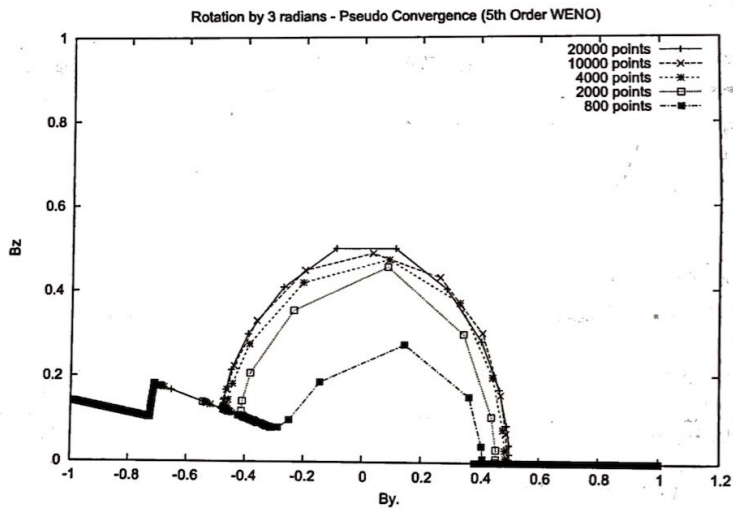
Figure 3.25: Variation of Solution with grid resolution (B_x - B_y plane)

Chapter 4
2D MHD - Numerical Implementation

The 2D equations of ideal MHD are obtained from the ideal MHD system, eq. (2.12), by considering gradients to exist only in the x and y directions. They can be expressed in the conservative form as [7]:

$$\frac{\partial \mathbf{u}}{\partial t} + \nabla.\mathcal{F} = 0 \tag{4.1}$$

where the flux is $\mathcal{F} = \mathbf{f}\hat{\mathbf{i}} + \mathbf{g}\hat{\mathbf{j}}$, $\mathbf{u} = [\rho \ \rho u \ \rho v \ \rho w \ B_x \ B_y \ B_z \ E]^T$ and

$$\mathbf{f(u)} = \begin{bmatrix} \rho u \\ \rho u^2 + P^* - B_x^2 \\ \rho uv - B_y B_x \\ \rho uw - B_z B_x \\ 0 \\ uB_y - vB_x \\ uB_z - wB_x \\ (E + P^*)u - B_x(\mathbf{u.B}) \end{bmatrix}, \ \mathbf{g(u)} = \begin{bmatrix} \rho v \\ \rho uv + -B_x B_y \\ \rho v^2 + P^* - B_y^2 \\ \rho vw - B_z B_y \\ vB_x - uB_y \\ 0 \\ vB_z - wB_y \\ (E + P^*)v - B_y(\mathbf{u.B}) \end{bmatrix} \tag{4.2}$$

As with the 1D system, the above equations are non-strictly hyperbolic and have non-convex flux functions. Additionally, while solving these equations numerically, it is imperative to ensure the solenoidal nature of the computed magnetic field. In 1D, this condition reduced to $B_x = constant$ and is satisfied by leaving out B_x from the evolution equations are treating it as a parameter. However, the treatment is more complicated in 2D and 3D. The magnetic field is required to satisfy:

$$\nabla.\mathbf{B} = 0 \Rightarrow \oint \mathbf{B}.\hat{\mathbf{n}}dS = 0 \Rightarrow \sum_{faces} \mathbf{B}.\hat{\mathbf{n}}\delta S = 0 \tag{4.3}$$

A number of methods have been developed to enforce this condition in numerical computations as discussed in section (2.5). In the present study, the 8-wave formulation developed in [3, 29] is used.

4.1 The 8-wave Formulation

The 8-wave formulation is derived from adding a source term proportional to the divergence of $\mathbf{B}$ to the governing equation (4.1). The modified equation can be derived from the basic equations of magnetohydrodynamics by *not* enforcing the condition that the divergence of $\mathbf{B}$ is zero and retaining terms containing $\nabla.\mathbf{B} = 0$ [3]. The aim is to obtain a symmetrizable form of

the MHD equations. Eq. (4.1) admits a zero eigenvalue which is non-physical in nature. The modified 8-wave formulation replaces this eigenvalue with u_n (the fluid velocity normal to the face) and thus all eigenvalues are symmetric about the fluid velocity. The modified governing equation is as follows:

$$\frac{\partial \mathbf{u}}{\partial t} + \nabla.\mathbf{F} = \mathbf{S} \qquad (4.4)$$

where $\mathbf{S} = -(\nabla.\mathbf{B})[0 \ \mathbf{B} \ \mathbf{u} \ \mathbf{u}.\mathbf{B}]^T$. The effect of the source term on the divergence of B can be seen by taking the divergence of all terms of the induction equation in eq. (2.12). Without the source term, this results in the constraint $\nabla.\mathbf{B} = \mathbf{0}$. If the initial conditions satisfy this condition, the computed solution should ideally satisfy it, assuming no errors in computations. However with the source term included, one obtains

$$\frac{\partial \rho \phi}{\partial t} + \nabla.(\rho \mathbf{u} \phi) = 0 \qquad (4.5)$$

where $\phi = \nabla.\mathbf{B}/\rho$. This describes the equation of the quantity ϕ which is being passively convected with the fluid. For the solution, ϕ is constant for all streaklines and since the initial and boundary conditions satisfy the zero divergence condition, the solution should also have zero divergence. Another way to interpret the effect of adding a source term is to observe that due to the convection equation, any finite value that the divergence of B may develop as the solution progresses will get convected away. However, it should be noted that the modified equations are no longer strictly conservative in nature. Ideally, when the divergence is zero, the modified and original equations are identical and thus, conservative. In numerical computations, the divergence will never be strictly zero and will have some value of the order of round-off errors. This will lead to slight errors in meeting shock jump conditions. It is expected that the effect on the solution will be negligible.

4.2   The 2D MHD Eigenstructure

The 8-wave formulation admits eight eigenvalues. For an arbitrary face with normal $\hat{n}$, the eigenvalues are as follows:

- $\lambda_e = u_n$ - entropy wave

- $\lambda_d = u_n$ - "divergence" wave

- $\lambda_s = u_n \pm c_s$ - left and right running slow waves

- $\lambda_a = u_n \pm c_a$ - left and right running Alfvén waves

- $\lambda_f = u_n \pm c_f$ - left and right running fast waves

where the wavespeeds are given by

$$c_a = B_n/\sqrt{\rho} \qquad (4.6)$$

$$c_{f,s}^2 = \frac{1}{2}[\frac{\gamma p + \mathbf{B}.\mathbf{B}}{\rho} \pm \sqrt{(\frac{\gamma p + \mathbf{B}.\mathbf{B}}{\rho})^2 - \frac{4\gamma p B_n^2}{\rho^2}}] \qquad (4.7)$$

and the subscript n denoted quantities normal to the interface. The eigenvectors for this modified system, as derived from the primitive variables ($\mathbf{w} = [\rho \ u \ v \ w \ B_x \ B_y \ B_z \ p]^T$), have been derived in [3] for the special case of the interface being normal to the x-axis. In the present study, the eigenvectors, in terms of the conserved variables, are derived by appropriately multiplying the eigenvectors in primitive form by the Jacobians of transformation relating conserved and primitive variables. Additionally, using the rotation matrices for transformation of the velocity and magnetic fields from Cartesian coordinates to face-normal and tangential coordinates and vice versa, the eigenvectors are derived for an arbitrary face.

4.3   Numerical Scheme

The governing equation, discretized in space is given as:

$$\frac{d\mathbf{u}_{ij}}{dt}V_{ij} + \sum_{faces} \mathbf{F}.\hat{n}dS = \mathbf{S}_{ij}V_{ij} \Rightarrow \frac{d\mathbf{u}_{ij}}{dt} = \text{Res}(i,j) \qquad (4.8)$$

where the residual is given by (for a quadrilateral cell)

$$\text{Res}(i,j) = \frac{-1}{V_{ij}}[\sum_{l=1}^{4} \mathbf{F}.\hat{n}_l dS_l + s_{ij}\sum_{l=1}^{4} \mathbf{B}.\hat{n}_l dS_l] \qquad (4.9)$$

where $\mathbf{s} = [0 \ \mathbf{B} \ \mathbf{u} \ \mathbf{u}.\mathbf{B}]^T$. The semi-discrete equation, as given by eq. (4.8) is marched in time using the multi-stage Runge-Kutta (RK) algorithm. The 1st order, 2nd and 3rd order TVD RK and 4th order RK time stepping are implemented and used in the present study. For the computation of the divergence term, the term s_{ij} is computed using the values at the cell center. The magnetic flux through the faces ($\mathbf{B}.\hat{n}_l dS_l$) are computed by taking the arithmetic average of the magnetic field at the cells on either side of the interface.

Currently, a high-resolution solver using ENO/WENO reconstruction based on the Roe's scheme is been implemented to compute the flux at the interface. A similar effort has been made in [3] which uses a weighted least-squares based reconstruction. The basic Roe's scheme is given by

$$\mathbf{F}.\hat{n}(\mathbf{u_L}, \mathbf{u_R}) = \frac{1}{2}[(\mathbf{F}.\hat{n}(\mathbf{u_L}) + \mathbf{F}.\hat{n}(\mathbf{u_R})) - \sum_{k=1}^{8} \mathbf{L}_k(\mathbf{u_R} - \mathbf{u_L})|\lambda_k|\mathbf{R_k}] \qquad (4.10)$$

To prevent the formation of expansion shocks, the Harten's entropy fix in the form used in [3] is implemented. It is observed that without this entropy fix, the solution computed is grossly erroneous and for many problems, negative pressures are encountered after a few iterations. The reconstruction of the flux is done via a characteristic decoupling and the approach outlined in section (3.4) is extended to multi-dimensions.

4.4 Results and Discussion

In the present study, the algorithm is validated for test cases which have become benchmark problems for 2D MHD on Cartesian meshes. Through these validation cases, a number of boundary conditions (outgoing, solid, periodic, specified free-stream) are developed. Representative results reported here include the Orszag-Tang vortex problem [7, 20, 32, 33], the cloud-shock interaction [32] and the fast rotor problem [34, 32, 33]. Unless mentioned otherwise, the domain in all problems as been taken to be a square of unit length. Aside for the problems reported here, the algorithm has also been tested on some hydrodynamic problems, since in the absence of a magnetic field, the MHD equations reduce to the Euler's equations. These test cases include the 2D Riemann problems as well as the oblique shock reflection problem. The initial conditions are specified in the following subsections in terms of the primitive variable vector $\mathbf{W} = [\rho,\ u,\ v,\ w,\ B_x,\ B_y,\ B_z,\ p]^T$.

4.4.1 Orszag-Tang Vortex Problem

The evolution of the Orszag-Tang vortex system is considered in this problem. It was proposed as a simple model to study significant features of supersonic MHD turbulence and tests the algorithm's robustness at handling the formation of shocks and multiple shock-shock interactions. The initial data consists of a superimposition of sinusoidal velocity and magnetic fields and the flow quickly transforms to a very complex structure with multiple interacting shocks. This test problem has become a benchmark for 2D algorithms and has been solved for in [7, 20, 32, 33] with slightly varying initial conditions (which are all topologically similar). In the present study, the initial conditions are as follows:
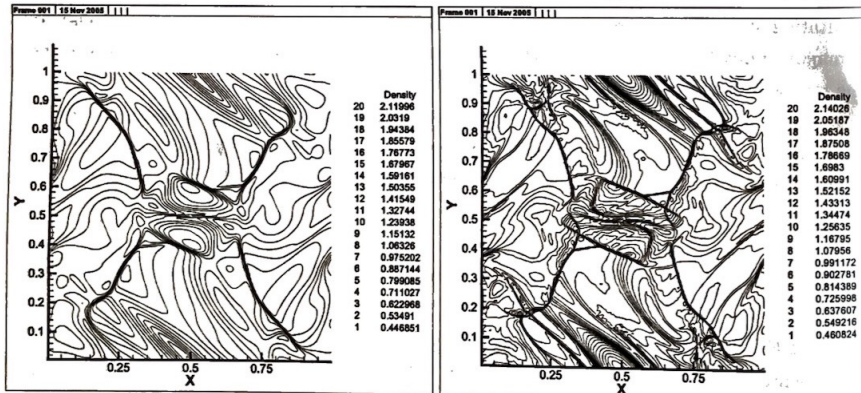

Figure 4.1: Orszag-Tang Vortex Problem - 1st Order Upwind and 5th Order WENO
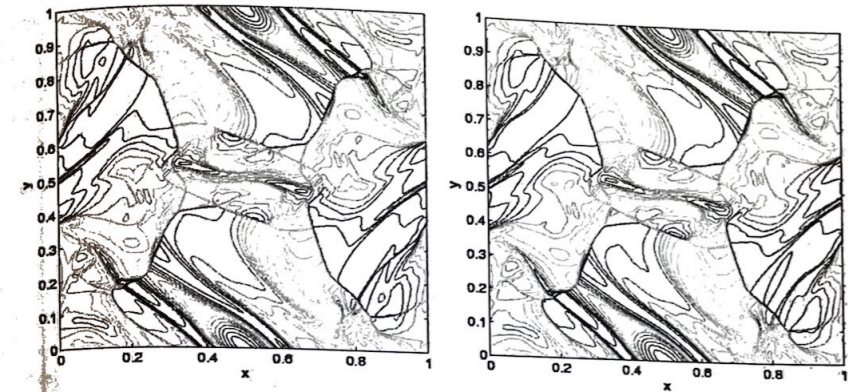

Figure 4.2: Orszag-Tang Vortex Problem - FLASH results and Deane & Lee's results [7]

$$\mathbf{W}_{initial} = [1.0,\ -sin(2\pi y),\ sin(2\pi x),\ 0,\ -sin(2\pi y)/\gamma,\ sin(4\pi x)/\gamma,\ 0,\ 1/\gamma]^T \quad (4.11)$$

with $\gamma = 1.67$. The boundary conditions are all periodic. The solution at time $t = 0.5$ is computed using a 200×200 grid. The computations were done using 1st order Roe (with 1st order time stepping), 2nd & 3rd order ENO (with 2nd order TVD RK time stepping) and 5th order WENO (with 3rd order TVD RK time stepping). Figure (4.1) shows the density contours obtained by using the 1st order upwind and 5th order WENO reconstructions. As is expected, the resolution of the solution increases as the spatial order is increased. However, the higher-order reconstructions also exhibit slight oscillations which are more pronounced on a coarser mesh and/or higher CFL than what can be seen here. Figure (4.2) shows the results presented in [7] which were obtained using the a staggered mesh, dimensionally-split algorithm and by using the FLASH code, developed and maintained by the Alliance Center for Astrophysical Thermonuclear Flashes at the University of Chicago (http://flash.uchicago.edu). Both these results were obtained using a 200×200 grid. A good agreement is seen with the between our results and those in [7]

4.4.2 Rotor Problem

The evolution of a dense, rotating fluid in an ambient, stationary fluid of lesser density is studied in this problem [34, 32, 33]. The initial conditions are identical to those specified in [32] as "Rotor problem 1". There is a disk of dense rotating fluid with $\rho = 10$, $u = -v_0(y-0.5)/r_0$ and $v = v_0(x-0.5)/r_0$ with a radius $r_0 = 0.1$ and $v_0 = 2$. The ambient fluid is at rest with $\rho = 1$ for $r > r_1 = 0.115$ ($r = \sqrt{(x-0.5)^2 + (y-0.5)^2}$). For the fluid in between ($r_0 < r < r_1$), linear density and angular speed profiles are provided with $\rho = 1 + 9f$, $u = -fv_0(y-0.5)/r$, $v =$
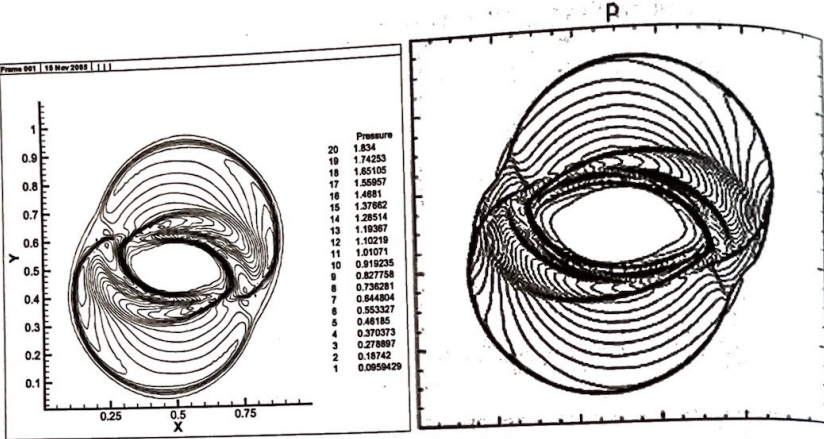
Figure 4.3: Rotor Problem (Pressure) - 3rd Order ENO and Toth's solution [32]

$fv_0(x - 0.5)/r$ where $f = (r_1 - r)/(r_1 - r_0)$. An uniform pressure and magnetic field exist throughout the domain ($p = 1$, $B_x = 5/\sqrt{4\pi}$) with $\gamma = 1.67$. Out-of-plane components of velocity and magnetic fields are zero. All boundaries were outgoing. The solution is obtained for a time level of 0.15. Figure (4.3) shows the pressure contours obtained using a 3rd order ENO scheme with 2nd order time stepping on a 100×100 grid and that obtained in [32] using a constrained transport/central difference based scheme on a 400×400 grid. The computed result show a good agreement with the results in [32]. The same problem, solved in [34, 33] has slightly different initial conditions. The results are qualitatively similar.

4.4.3 Cloud Shock Interaction

This problem studies the interaction of a high density cloud, moving at supersonic speeds (approximately 8.7 Mach), and a stationary shock [32]. The initial conditions consist of a stationary discontinuity which is a fast shock combined with a rotational discontinuity in B_z. The left and right states are given by:

$$\mathbf{W}_L = [3.87\ 0\ 0\ 0\ 0\ 2.18\ -2.18\ 167.35], \quad \mathbf{W}_R = [1\ -11.25\ 0\ 0\ 0\ 0.56\ 0.56\ 1] \quad (4.12)$$

with $\gamma = 1.67$. The discontinuity lies at $x = 0.6$. Superimposed on these initial conditions is a high density circular cloud with $\rho = 10$, $p = 1.0$ centered at $x = 0.8$, $y = 0.5$ with a radius 0.15, moving leftwards at the same velocity as the ambient gas. The right boundary is a supersonic inflow boundary with the conditions specified as $\mathbf{W}_R$ while all other boundaries are outgoing. Figure (4.4) shows the density contours and magnetic field lines obtained from a 2nd order ENO scheme on a 200×200 grid. The computed results are compared with those obtained by [32]. Figure (4.5) shows the results obtained in [32] using a constrained transport/central difference

type scheme on a 400×400 grid. A logarithmic gray-scale plot (white - minimum, black - maximum) of density and the magnetic field lines in the x-y plane are shown respectively. The solution is obtained at a time level of 0.06. A good agreement is seen between the two sets of results although the resolution of Toth's results is better (especially ahead (leftwards) of the high density cloud) due to a finer grid.
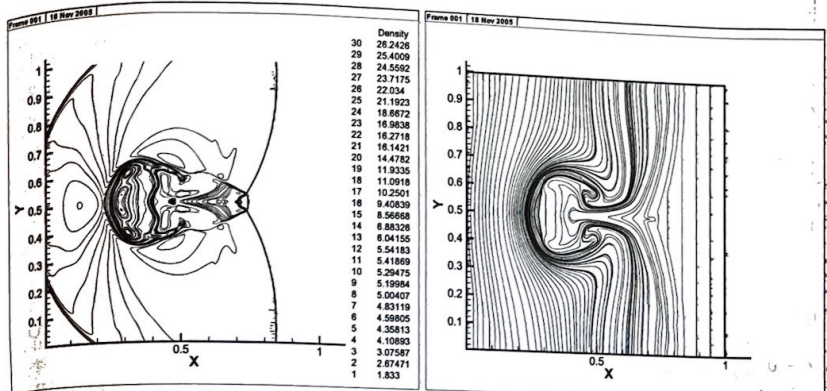

Figure 4.4: Cloud Shock Interaction (Density and magnetic field line) - 2nd Order ENO
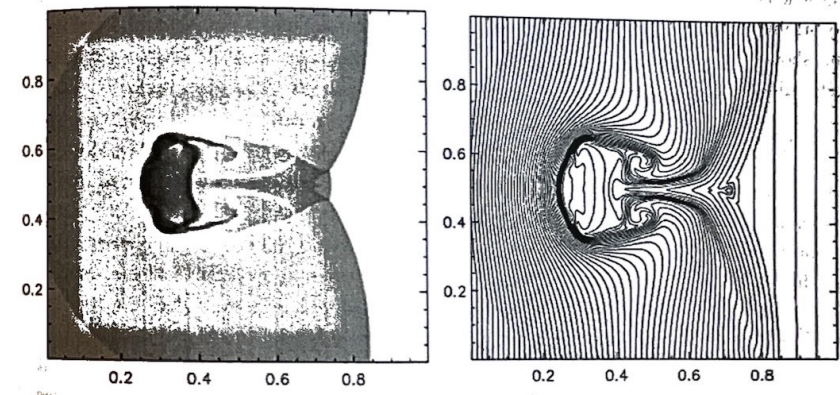

Figure 4.5: Cloud Shock Interaction (Density and magnetic field lines) - Toth's solution [32]

Chapter 5
Conclusions

In the present study, a characteristic-based algorithm is constructed using ENO/WENO class of schemes and validated on benchmark problems in 1D ideal MHD. The results indicate that while the higher order non-oscillatory schemes show considerably better resolution compared to the 1st order scheme for the MHD equations, they exhibit some spurious oscillations. To address this issue, a comprehensive study is made of the characteristic behavior of the ideal MHD equations, when solved using higher order WENO schemes. While oscillatory behavior by WENO schemes has also been reported in literature, a solution-dependent monotonicity-preserving limiting technique has been proposed to alleviate this problem. The efficacy and the necessity of these MP limits is studied for the characteristic fields of ideal MHD. The 2×2 rotationally degenerate system, suggested as a prototype for the Alfvén mode, is solved with higher order WENO schemes and it is seen that no oscillations occur at such high orders, across all types of waves. This indicates that the MP limits are not necessary on the Alfvén mode in the ideal MHD equations because of the mathematical similarities between the rotationally degenerate system and the Alfvén waves. Subsequently, the 3×3 model system, which is representative of the ideal MHD equations by modeling the right-running waves, is solved using the higher order WENO schemes. Planar cases are solved to study the behavior of the slow and fast magnetosonic modes and these modes are seen to be susceptible to spurious oscillations. The MP limits are applied which alleviate these oscillations with varying degrees of success. The observation from the rotationally degenerate system (that the Alfvén mode does not need the limiting procedures) is verified using non-planar modifications of the planar problems so as to yield an additional wave of the Alfvén family. It is seen that solutions computed with and without the MP limits on the the Alfvén mode coincide, thus reiterating the previous observation. These conclusions are extended to the ideal MHD system and a characteristic-based algorithm is developed using higher order ENO/WENO schemes with the limiting procedure applied on the magnetosonic and entropy modes. Two benchmark problems are solved and it is seen that the limiting procedure is extremely effective in removing the spurious oscillations. Non-planar modifications of the Brio & Wu's shock tube problem are solved and it is verified that the conclusions about the Alfvén mode extends to the ideal MHD equations. The selective use of MP limits has resulted in a significant saving in the computational cost for the 1D problems studied here and it is expected that this will be further amplified for multi-dimensional problems.

Another thrust of the present study is to understand the wave nature of ideal MHD which has been investigated extensively in literature. Inspite of a lot of efforts in this area in the past couple of decades, discrepancies still persist in the various conclusions arrived at by various researchers and the question of shock admissibility has still not been resolved. The relevance of ideal MHD to practical problems has also come under doubt. These issues are connected with the issues of pseudo-convergence seen for all Godunov-type methods while computing solutions for a class of slightly-non-planar initial conditions. The problems regarding psuedo-convergence are studied using the algorithm developed in the present study.

Simultaneously, a high-resolution solver using the ENO/ WENO reconstruction based on the Roe scheme is implemented for the 2D equations. The solution and flux are reconstructed via characteristic decoupling. The 2nd & 3rd order ENO and 5th order WENO spatial reconstruction and 2nd & 3rd order TVD Runge-Kutta and 4th order Runge-Kutta time-stepping are implemented, apart from the basic 1st order scheme. The code is validated for a number of benchmark problems involving cartesian grids. It is seen that though the solutions obtained show good agreement with those in literature, spurious oscillations occur which limit the use of higher order schemes. Thus, one natural direction of future work is the extension of the MP limits to the 2D algorithm. However, a significant drawback in this would be the tremendous increase in the computational costs, even with a refined use, as proposed in this report. An estimate of this increase can be obtained by extrapolating the CPU times tabulated for 1D problems in this report. Presently, the algorithm has been for problems on Cartesian meshes only and thus needs to be extended to non-Cartesian meshes to solve truly multi-dimensional problems. Once the code is validated on body-fitted grids and its performance evaluated for all kinds of boundary conditions, it can be used to carry out blunt body computations, whose results are likely to be of relevance to studying flow past bodies at hypersonic velocities.

References

1. Sutton G. W., Sherman A., *Engineering Magnetohydrodynamics*, McGraw Hill, New York, 1965

2. Bittencourt J.A., *Fundamentals of Plasma Physics*, Springer - Verlag, New York, 2004

3. Powell K.G., Roe P.L., et. al, *A Solution-Adaptive Upwind Scheme for Ideal Magnetohydrodynamics*, Journal of Computational Physics, **154**, 1999, 284 - 309

4. J.S. Shang, *Recent Research in Magneto-aerodynamics*, Progress in Aerospace Sciences, **37**, 2001, 1 - 20

5. Brio M., Wu C.C., *An Upwind Differencing Scheme for the Equations of Ideal Magnetohydrodynamics*, Journal of Computational Physics, **75**, 1988, 400 - 422

6. Zachary A.L., Colella P.A., 1992, *A Higher-Order Godunov method for the Equations of Ideal Magnetohydrodynamics*, Journal of Computational Physics, **95**, 1992, 341 - 347

7. Lee D., Deane A., *A Numerical Implementation of Magnetohydrodynamics using a Staggered Mesh with High Order Godunov Fluxes*, Project Final Report AMSC 663-664, University of Maryland, College Park, Maryland, 2004

8. Kennel C.F., Blandford R.D., Coppi P., *MHD intermediate shock discontinuities. Part 1. Rankine-Hugoniot conditions*, Journal of Plasma Physics, **42** (2), 1989, 299 - 319

9. Wu C.C., *The MHD Intermediate Shock Interaction with an Intermediate Wave: Are Intermediate Shocks Physical*, Journal of Geophysical Research, **93**, 1988, 987 - 999

10. Wu C.C., *Formation, Structure and Stability of MHD Intermediate Shocks*, Journal of Geophysical Research, **95**, 1990, 8149 - 8175

11. Barmin A.A., Kulikovskiy A.G., Pogorelov N.V., *Shock-Capturing Approach and Non-Evolutionary Solutions in Magnetohydrodynamics*, Journal of Computational Physics, **126**, 1996, 77 - 90

12. Myong R.S., Roe P.L., *On Godunov-type schemes for Magnetohydrodynamics*, Journal of Computational Physics, **147**, 1998, 545 - 567

13. Roe P.L., Balsara D.S., *Notes on the Eigensystem of Magnetohydrodynamics*, SIAM Journal of Applied Mathematics, **56** (1), 1996, 57 - 67

14. Cargo P., Gallice G., *Roe Matrices for Ideal MHD and Systematic Construction of Roe Matrices for Systems of Conservation Laws*, Journal of Computational Physics, **136**, 1997, 446 - 466

15. Shu C.W., Osher S., *Efficient Implementation of Essentially Non-Oscillatory Shock-Capturing Schemes*, Journal of Computational Physics, **77**, 1988, 439 - 471

16. Shu C.W., Osher S., *Efficient Implementation of Essentially Non-Oscillatory Shock-Capturing Schemes, II*, Journal of Computational Physics, **83**, 1989, 32 - 78

17. Shu C.W., Osher S., *Essentially Non-Oscillatory and Weighted Essentially Non-Oscillatory Schemes for Hyperbolic Conservation Laws*, ICASE report 97-65, 1997

18. X.D. Liu, S. Osher, T. Chan, *Weighted Essentially Non-oscillatory Schemes*, Journal of Computational Physics, **115**, 1994, 200 - 212

19. Jiang G.S., Shu C.W., *Efficient Implementation of Weighted ENO Scheme*, Journal of Computational Physics, **126**, 1996, 202 - 228

20. Jiang G.S., Shu C.W., *A High Order WENO Finite Difference Scheme for the Equations of Ideal Magnetohydrodynamics*, Journal of Computational Physics, **150**, 1999, 561 - 594

21. Torrilhon M., *Non-uniform convergence of finite-volume schemes for Riemann problems of Ideal Magnetohydrodynamics*, Journal of Computational Physics, **192**, 2003, 73 - 94

22. Torrilhon M., Balsara D.S., *High Order WENO schemes: investigations on non-uniform convergence for MHD Riemann problems*, Journal of Computational Physics, **201**, 2004, 586 - 600

23. D.S. Balsara, C.W. Shu, *Monotonicity Preserving Weighted Essentially Non-Oscillatory Schemes with Increasingly High Order of Accuracy*, Journal of Computational Physics, **160**, 2000, 405 - 452

24. A. Suresh, H.T. Huynh, *Accurate Monotonicity Preserving Scheme with Runge-Kutta time-stepping*, Journal of Computational Physics, **136**, 1997, 83 - 99

25. Myong R.S., Roe P.L., *Shock Waves and Rarefaction Waves in Magnetohydrodynamics. Part 1. A model system*, Journal of Plasma Physics, **58** (3), 1997, 485 - 519

26. Myong R.S., Roe P.L., *Shock Waves and Rarefaction Waves in Magnetohydrodynamics. Part 2. The MHD system*, Journal of Plasma Physics, **58** (3), 1997, 521 - 552

27. H. Freistuhler, E.B. Pitman, *A Numerical Study of a Rotationally Degenerate Hyperbolic System. Part I. The Riemann Problem*, Journal of Computational Physics, **100**, 1992, 306 - 321

28. Falle S.A.E.G., Komissarov S.S., *On the inadmissibility of non-evolutionary shocks*, Journal of Plasma Physics, **65** (1), 2001, 29 - 58

29. Powell K.G., *A Riemann Solver for Ideal MHD That Works in More Than One Dimension*, ICASE Report 94 - 24, 1994

30. Lax P.D., Liu X.D., *Solution of Two Dimensional Riemann Problems of Gas Dynamics by Positive Schemes*, SIAM Journal of Scientific Computing, **19** (2), 1998, 319 - 340

31. Aslan N., Kammash T., *A Riemann Solver For the Two-Dimensional MHD Equations*, International Journal for Numerical Methods in Fluids, **25**, 1997, 953 - 957

32. Toth G., *The $\nabla.B = 0$ Constraint in Shock Capturing Magnetohydrodynamics Codes*, Journal of Computational Physics, **161**, 2000, 605 - 652

33. Londrillo P., Del Zanna L., *On the divergence-free condition in Godunov-type schemes for ideal magnetohydrodynamics: the upwind constrained transport method*, Journal of Computational Physics, **195**, 2004, 17 - 48

34. Li S., *An HLLC Riemann Solver for Magnetohydrodynamics*, Preprint submitted to Elsevier Science, 2003

35. Brackbill J.U., Barnes D.C., *The Effect of Non-Zero $\nabla.B$ on the Numerical Solution of Magnetohydrodynamic Equations*, Journal of Computational Physics, **35**, 1980, 426 - 430

Acknowledgments